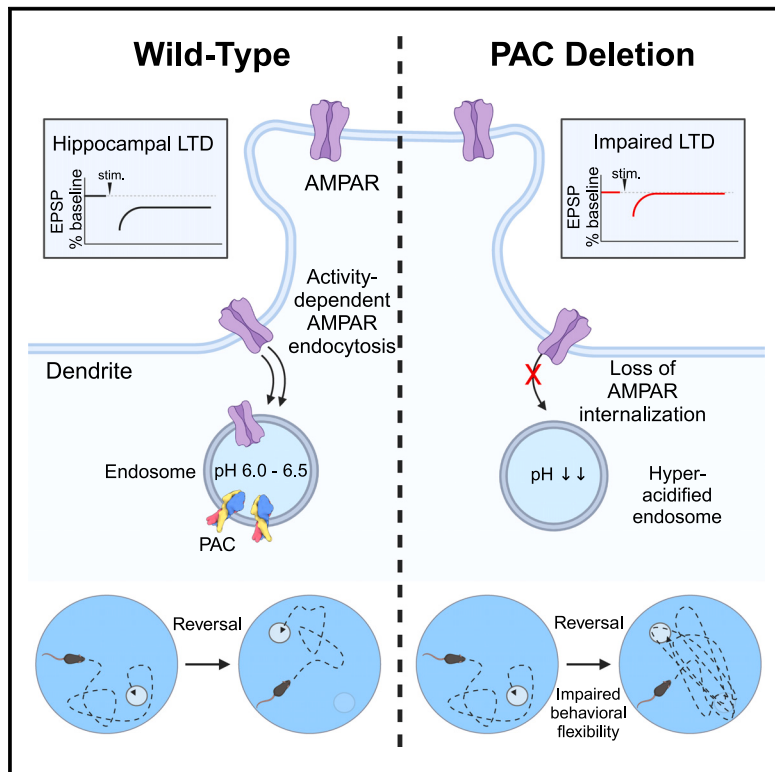


## Loss of the proton-activated chloride channel in neurons impairs AMPA receptor endocytosis and LTD via endosomal hyper-acidification

### Graphical abstract



### Authors

Kevin H. Chen, Junhua Yang, Bian Liu, ..., Shuying Sun, Richard Huganir, Zhaozhu Qiu

### Correspondence

zhaozhu@jhmi.edu

### In brief

Chen et al. report that the proton-activated chloride (PAC) channel is a regulator of endosomal pH in neurons and is involved in the expression of hippocampal LTD by mediating activity-dependent AMPAR endocytosis.

### Highlights

- PAC localizes to endosomes and regulates luminal pH in neurons
- Direct imaging of AMPAR endocytosis in live neurons with a HaloTag-GluA2 approach
- Activity-dependent AMPAR endocytosis requires proper endosomal pH homeostasis
- Neuronal PAC deletion impairs hippocampal LTD and adaptive behavior in mice



## Article

# Loss of the proton-activated chloride channel in neurons impairs AMPA receptor endocytosis and LTD via endosomal hyper-acidification

Kevin H. Chen,<sup>1</sup> Junhua Yang,<sup>1,2</sup> Bian Liu,<sup>3</sup> Chaohua Jiang,<sup>1</sup> Nicholas Koylass,<sup>1</sup> Zhe Zhang,<sup>1</sup> Shuying Sun,<sup>1,3</sup> Richard Huganir,<sup>3</sup> and Zhaozhu Qiu<sup>1,3,4,5,\*</sup>

<sup>1</sup>Department of Physiology, Johns Hopkins University School of Medicine, Baltimore, MD 21205, USA

<sup>2</sup>Department of Veterinary Integrative Biosciences, College of Veterinary Medicine and Biomedical Sciences, Texas A&M University, College Station, TX 77843, USA

<sup>3</sup>Solomon H. Snyder Department of Neuroscience, Johns Hopkins University School of Medicine, Baltimore, MD 21205, USA

<sup>4</sup>Department of Neurosurgery, Johns Hopkins University School of Medicine, Baltimore, MD 21205, USA

<sup>5</sup>Lead contact

\*Correspondence: zhaozhu@jhmi.edu

<https://doi.org/10.1016/j.celrep.2025.115302>

## SUMMARY

Hippocampal long-term potentiation (LTP) and long-term depression (LTD) are forms of synaptic plasticity, thought to be the molecular basis of learning and memory, dependent on dynamic  $\alpha$ -amino-3-hydroxy-5-methyl-4-isoxazolepropionic acid receptor (AMPAR) trafficking. Alteration of endosomal pH negatively affects synaptic transmission and neural development, but it is unclear how pH is involved in AMPAR trafficking. We show that the proton-activated chloride (PAC) channel localizes to early and recycling endosomes in neurons and prevents endosome hyper-acidification. Loss of PAC reduces AMPAR endocytosis during chemical LTD in primary neurons, while basal trafficking and LTP are unaffected. Pyramidal neuron-specific PAC knockout mice have impaired hippocampal LTD, but not LTP, and perform poorly in the Morris water maze reversal test, exhibiting impaired behavioral adaptation. We conclude that proper maintenance of endosomal pH by PAC in neurons is important during LTD to regulate AMPAR trafficking in a manner critical for animal physiology and behavior.

## INTRODUCTION

Synaptic plasticity, the ability of individual synapses to modulate their connective strength based on patterns of neural activity, is thought to be the molecular basis of neural plasticity and underlies complex behaviors such as learning and memory.<sup>1</sup> Long-term potentiation (LTP) and long-term depression (LTD) are well-established models of long-lasting synaptic plasticity and, at glutamatergic synapses, involve the regulation of post-synaptic  $\alpha$ -amino-3-hydroxy-5-methyl-4-isoxazolepropionic acid receptors (AMPARs) either through dynamic AMPAR trafficking at the post-synaptic membrane or modulation of channel properties and binding proteins.<sup>2</sup> AMPARs can be trafficked through synapses, extrasynaptic membranes, and the endocytic pathway to regulate the strength of glutamatergic synapses. LTP occurs by enhancing the delivery of AMPARs to the post-synaptic membrane from extrasynaptic and endosomal membranes.<sup>3</sup> Conversely, LTD reduces AMPAR content at the post-synaptic density (PSD) through diffusion and endocytosis, followed by either sequestration in recycling endosomes or degradation through the endolysosomal pathway.<sup>4</sup> While many mechanisms are involved in synap-

tic plasticity, the expression of excitatory synaptic plasticity through AMPARs is inextricably linked to the endosomal pathway.<sup>5,6</sup>

Disrupted endosomal function, due to endosomal alkalinization or hyper-acidification, can impair synaptic plasticity. Indeed, direct endosomal alkalinization by an optogenetically activated proton leak channel abolishes LTD in the cerebellum.<sup>7</sup> Consistent with these findings, aberrations in AMPAR trafficking and synaptic plasticity have been shown to occur during genetic ablation of various endosomal adaptor proteins that interact with AMPARs, such as protein interacting with C kinase 1 (PICK1),<sup>8,9</sup> synaptotagmin-3,<sup>10</sup> glutamate receptor-interacting protein (GRIP)-associated protein 1,<sup>11</sup> or the Rab family of small guanosine triphosphate hydrolases, which compartmentalize endosomal membranes and designate endosomal identity.<sup>12,13</sup> Moreover, dysfunction of multiple ion transporters, including the V-type ATPase, chloride transporters (CLCs), and endosomal sodium-proton exchangers (NHEs), which regulate ion homeostasis and pH in the endosomal lumen, are associated with neuropsychological impairments, including Alzheimer's disease, intellectual disability, and autism spectrum disorder.<sup>14–16</sup> Thus, proper



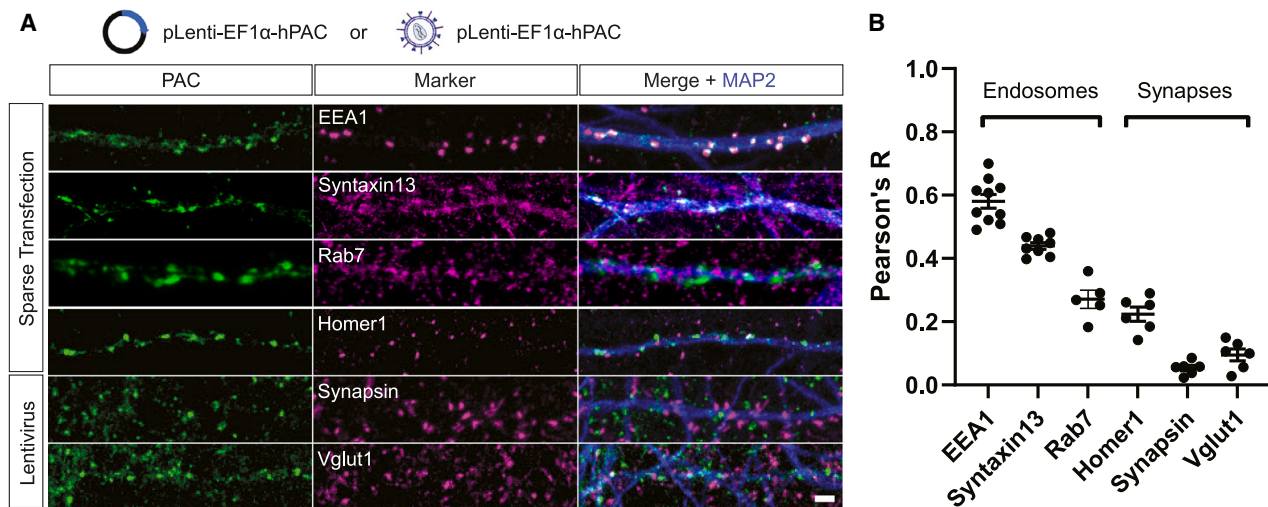


**Figure 1. PAC localizes to endosomes in the dendrites of hippocampal neurons**

(A) Co-immunofluorescence labeling of PAC and cellular markers in rat primary hippocampal neurons. Sparse transfection of PAC was used to visualize post-synaptic neurons, and lentiviral transduction of PAC was used to visualize pre-synaptic markers. Scale bar: 2  $\mu$ m.  
(B) Quantification (mean  $\pm$  SEM) of colocalization using Pearson's R for PAC and various markers. PAC signal is correlated with EEA1 and Syntaxin13 signals and is not closely correlated with Rab7, Homer1, Synapsin, and Vglut1 signals. Points represent 1 neuron.

synaptic function depends on the trafficking and signaling roles of the endolysosomal system. However, little is known how endosome hyper-acidification directly affects AMPAR trafficking during synaptic plasticity.

Through an unbiased screen, we have recently revealed the molecular identity of the proton-activated chloride (PAC) channel.<sup>17</sup> PAC (encoded by *Pacc1*, also known as TMEM206) is ubiquitously expressed and primarily localized to endosomes in various cell lines and is enriched in several organs, including the brain. Endosomal PAC becomes activated in the low-pH environment of endosomes and functions as a chloride release channel to lower luminal  $[Cl^-]$  and prevent hyper-acidification.<sup>18</sup> In macrophages, PAC also regulates macropinosome volume resolution.<sup>19</sup> Under pathological acidosis conditions, the plasma membrane PAC channel has been shown to mediate acid-induced cytotoxicity and increase susceptibility to ischemic stroke in mice.<sup>17,20</sup> Despite much progress in studying the biophysical and cellular roles of PAC,<sup>21,22</sup> its function has not been established in the context of AMPAR trafficking and synaptic plasticity in the brain, where it is highly expressed.

Here, we developed a chemogenetic approach to longitudinally visualize AMPAR endocytosis and determined that loss of functional PAC channels in neurons impairs endosomal pH homeostasis and disrupts the AMPAR internalization pathway required for hippocampal LTD. Moreover, we found that PAC impairment causes changes in animal behavior during tasks requiring behavioral flexibility, which is the ability to adapt to changing environments. PAC deletion specifically altered activity-dependent AMPAR endocytosis without affecting LTP or basal AMPAR trafficking, revealing a distinct role of PAC-dependent endosomal acidification in synaptic plasticity.

## RESULTS

### PAC localizes to early and recycling endosomes but not synaptic vesicles

PAC localization in neurons has not been established. To explore the subcellular location of PAC, we transfected primary hippocampal rat neurons with a human isoform of PAC (hPAC) and stained neurons using a validated antibody developed previously.<sup>18</sup> Neurons co-expressed cytosolic mVenus and were immunolabeled with anti-hPAC and microtubule-associated protein 2 (MAP2) antibodies. Axons and dendrites were distinguished through cellular morphology and fluorescence signals from mVenus and MAP2, a dendrite marker, where axons are MAP2 negative/mVenus positive, and dendrites are MAP2 positive. Using this approach, we observed PAC puncta in the cell soma, axons, and dendrites (Figure S1A).

In dendrites, PAC mainly colocalizes with the early endosome marker early endosome antigen 1 (EEA1) and the recycling endosome marker syntaxin13 (Figures 1A and 1B). PAC did not strongly localize to the late endosome protein Rab7, consistent with previous reports of PAC localization in other cell types. PAC does not localize to the post-synaptic density (PSD) marked by Homer1 (Figures 1A and 1B) but is positioned adjacent to the PSD, reminiscent of endocytic zones.<sup>23</sup> To label presynaptic proteins, we used lentiviral transduction of hPAC with a high transduction efficiency to express PAC in nearly all neurons but did not find PAC colocalization with pre-synaptic synapsin1 or with Vglut1-containing synaptic vesicles (Figures 1A and 1B). These results indicate that PAC localizes mainly to early and recycling endosomes in dendrites but not presynaptic boutons.

In addition to rat primary hippocampal neurons, we also investigated PAC localization in mouse primary hippocampal neurons and human i3 induced pluripotent stem cell-derived

neurons (iPSNs), the latter of which allowed us to examine the endogenous expression of PAC in human cells (Figure S1). Consistent with our data from rat neurons, PAC in mouse hippocampal neurons colocalizes with EEA1 and syntaxin13 but does not localize to the PSD protein PSD-95 or lysosome-associated membrane protein 2 (LAMP2) (Figure S1B). In human iPSNs, we detected endogenous PAC expression and colocalization with EEA1 (Figures S1C and S1D). We validated the staining specificity by knocking down endogenous PAC with clustered regularly interspaced short palindromic repeats interference (CRISPRi) and single-guide RNAs (sgRNAs) targeting its transcriptional start site, which abolished PAC mRNA levels and immunoreactivity in PAC knockdown (KD) neurons (Figures S1C and S1D). In agreement with previous reports of PAC localization, our results demonstrate that PAC localizes to early and recycling endosomes but not to synapses, synaptic vesicles, late endosomes, or lysosomes.

#### PAC regulates endosomal pH in neurons

We assessed the role of PAC in primary hippocampal and cortical neurons by expressing either control short hairpin RNA (shRNA) or PAC-specific shRNA to generate control and PAC KD neurons, respectively.<sup>24</sup> To further validate our PAC-specific shRNA, we developed a PAC antibody targeting the rodent PAC isoform and used western blotting to measure total PAC levels (Figure S2). Consistently, PAC protein was markedly reduced in PAC KD neurons compared to control neurons. PAC regulates endosomal pH by controlling luminal Cl<sup>-</sup> levels in several cancer cell lines, but this has not been explored in neurons. To measure endosomal pH in primary neurons, we used ratiometric pHluorin (RpH), a GFP mutant with two pH-dependent excitation peaks (405 nm/488 nm), where the ratio of these peaks is proportional to ambient pH.<sup>25</sup> To target RpH to endosomes, we fused the protein to the extracellular domain of the transferrin receptor (TfR) to generate a TfR-RpH fusion protein, which colocalizes with PAC in endosomes (Figures 2A and 2B). TfR-RpH fluorescence ratios of endosomes in hippocampal neurons co-expressing control or PAC shRNAs were measured first under physiological conditions in artificial cerebrospinal fluid (ACSF). Then, neurons were treated with pH calibration solutions containing the ionophore monensin, which equilibrates H<sup>+</sup> ions across cellular membranes (Figure 2C). As expected, the endosomal 405/488 nm excitation ratio decreased as pH decreased from 7.5 to 5.5. Fluorescence intensities of endosomes under the pH calibration solutions were plotted to generate a standard curve, which was used to calculate the physiological pH of endosomes measured in ACSF. We observed a significant decrease in endosomal pH in PAC KD (pH 5.997 ± 0.030) cells compared to the control (pH 6.493 ± 0.0785) (Figure 2D), indicating that PAC prevents hyper-acidification in neuronal endosomes.

To determine which functional domains of the PAC channel are necessary for regulating endosomal pH, we employed a molecular replacement strategy where hippocampal neurons were transfected with an shRNA targeting PAC plus shRNA-resistant cDNA of either wild-type (WT) hPAC, the endocytosis-defective mutant Y10A/L13A (YLAA), or the channel-dead mutant K319A (Figure 2D). WT and K319A PAC colocalized with endosomes, whereas the YLAA mutant was broadly distributed at the plasma

membrane (Figure S3A). Whole-cell patch-clamp recordings from K319A-expressing neurons revealed a large reduction in PAC chloride channel activity (Figure S3B). Overexpression of WT hPAC in PAC shRNA-transfected neurons increased endosomal pH (pH 6.406 ± 0.070), thereby rescuing the hyper-acidification phenotype. However, neither the YLAA (pH 6.104 ± 0.112) nor the K319A (pH 5.951 ± 0.065) mutant rescued endosomal pH in PAC KD neurons. These results demonstrate that PAC prevents endosomal hyper-acidification and that endosomal pH regulation depends on the proper localization and activity of the channel.

#### PAC does not affect AMPAR trafficking in unstimulated neurons or during chemical LTP

The phenotype in PAC KD neurons provides a rare opportunity to examine the potential effects of endosomal hyper-acidification on neuronal function, which has not been extensively explored. PAC KD did not disrupt the expression levels of many membrane and endosomal proteins in primary neurons (Figure S2). Protein levels of Na/K-ATPase, GluA1, GluA2, PSD-95, Homer1, synaptophysin, Rab5, Rab7, and Rab11 were normal in PAC KD neurons, indicating that PAC is not essential in regulating the expression of these synaptic and endosomal proteins under basal conditions. We have reported previously that PAC is involved in the endocytosis of TfR in cancer cell lines, altering surface expression and internalization dynamics.<sup>18</sup> To assess whether PAC is important for the proper surface expression of transmembrane proteins, we used surface biotinylation and streptavidin-mediated isolation of surface protein. We found that, in PAC KD neurons, surface levels of Na/K-ATPase, TfR, GluA2, and mGluR5 were unchanged compared to control neurons (Figures S2C and 3G), indicating that basal surface expression of many membrane proteins is unaltered by PAC deletion. This also suggests that mechanisms involved in TfR trafficking are different in immortalized cells compared to post-mitotic neurons.

We then assessed whether regulation of endosomal pH by PAC is functionally relevant for AMPAR trafficking in live neurons. To address this, we used control or PAC KD neurons co-expressing superecliptic pHluorin (SEP) tagged to the GluA2 AMPAR subunit (SEP-GluA2), a widely used tool to track AMPAR dynamics at dendritic spines, and measured AMPAR trafficking dynamics during basal conditions and chemical LTP (cLTP). We first employed fluorescence recovery after photo-bleaching (FRAP) to measure the lateral diffusion of SEP-GluA2 within dendritic spines. Spine SEP-GluA2 FRAP had an estimated time constant ( $\tau$ ) of 4.469 min for control neurons and 3.856 min for PAC KD neurons, which were comparable to previously reported values<sup>26</sup> (Figures 3A and 3B). To measure AMPAR delivery to dendritic spines during cLTP, we induced cLTP with glycine treatment and measured SEP-GluA2 intensity in dendritic spines during a 60-min period. As expected, spines of control neurons underwent a rapid fluorescence intensity increase upon glycine stimulation, which was maintained for 50 min. PAC KD neurons also showed a similar increase in SEP intensity throughout the experiment compared to controls (Figures 3C–3E). Interestingly, we observed a slight increase in trafficking kinetics for PAC KD neurons in both FRAP and cLTP experiments, but these changes were not statistically significant.

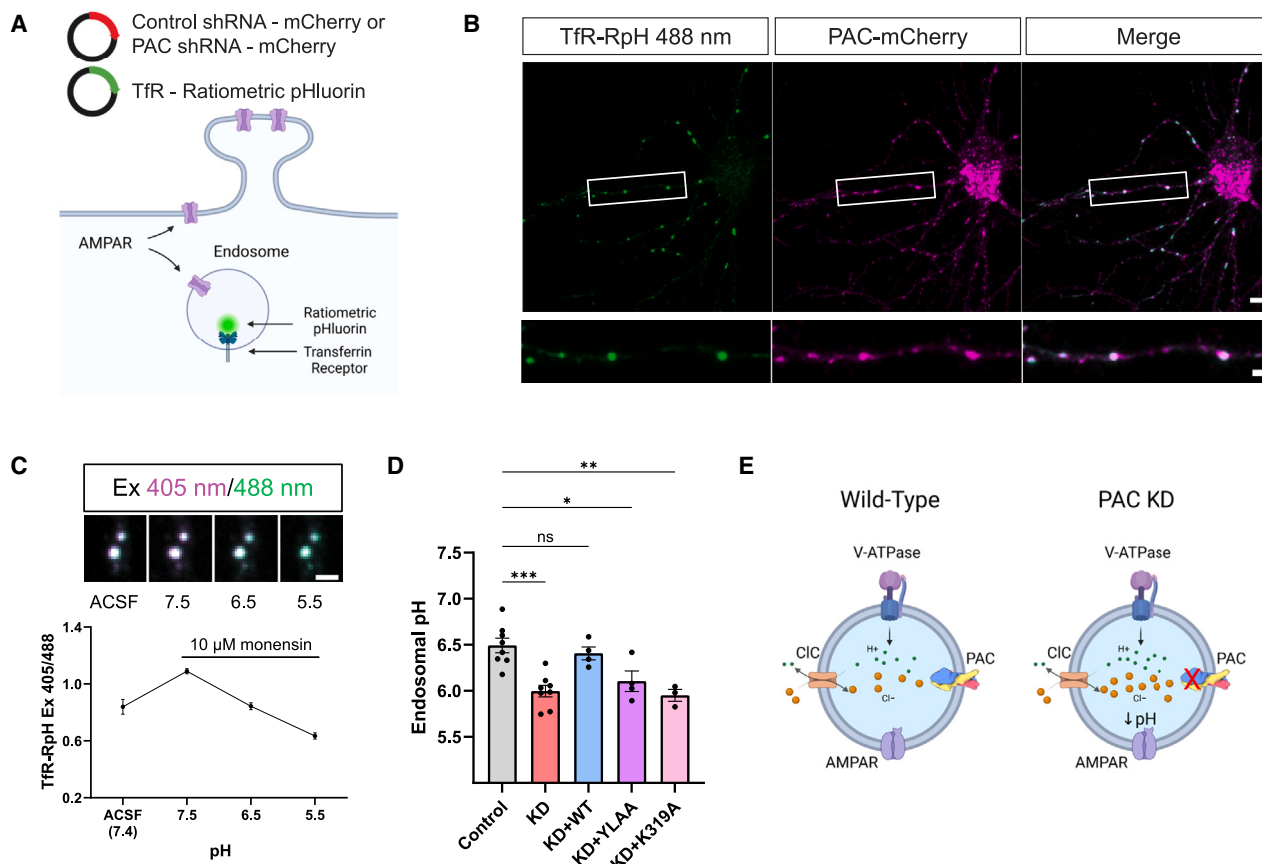


**Figure 2. PAC regulates endosomal pH in dendrites**

(A) Schematic of the ratiometric endosomal pH reporter TfR-RpH (transferrin receptor-ratiometric pHluorin) and co-transfection with control or PAC shRNA.

(B) Representative live neuron expressing the TfR-RpH pH reporter and colocalization with PAC. Scale bars: top, 10  $\mu$ m; bottom, 2  $\mu$ m.

(C) Fluorescence intensity measurements of individual endosomes under basal conditions and in pH 7.5–5.5 calibration buffers. Scale bar: 2  $\mu$ m.

(D) Ratiometric measurement of endosomal pH in neurons treated with control shRNA (ctrl, 6.475  $\pm$  0.063, n = 58), PAC shRNA (KD, 6.021  $\pm$  0.044, n = 68), or KD plus PAC WT (KD+WT, 6.391  $\pm$  0.073, n = 50), PAC YLAA mutant (KD+YLAA, 6.050  $\pm$  0.091, n = 47), or PAC K319A mutant (KD+K319A, 6.049  $\pm$  0.088, n = 47). Points represent one experiment, and n represents neurons. Error bars represent mean  $\pm$  SEM. two-way ANOVA with Tukey correction for multiple comparisons.

\*\*\*p < 0.001, \*\*p < 0.01, \*p < 0.05; ns, not significant.

(E) Model depicting how PAC regulates endosomal pH through pH-dependent chloride efflux.

Overall, PAC and endosomal hyper-acidification do not appear to be involved in the lateral mobility of AMPARs in unstimulated and glycine-stimulated neurons.

#### Activity-dependent AMPAR internalization is impaired during chemical LTD in PAC KD neurons

We next measured AMPAR internalization during chemical LTD (cLTD) using N-methyl-D-aspartic acid (NMDA) treatment. Due to confounding changes in intracellular pH caused by NMDA administration, SEP-GluA2 cannot faithfully measure internalization of AMPARs.<sup>27</sup> Instead, we employed a surface biotinylation assay following the cLTD stimulus to compare surface (sGluA2) versus total (tGluA2) levels of the AMPAR subunit GluA2 in control and PAC KD neurons. Using this approach, we observed an ~30% decrease in sGluA2 expression following NMDA treatment in control shRNA-treated cortical neurons (Figure 3F). Interestingly, PAC KD neurons failed to internalize GluA2 after

NMDA stimulation (Figure 3G). As a control, we measured tGluA2 levels (Figure 3H), which were unchanged by NMDA treatment.

Following LTD induction, AMPARs are transported to the early endosome and then to the late endosome via the AP-2 and AP-3 adaptor complexes, respectively.<sup>5</sup> To assess which step of AMPAR internalization is impaired in PAC KD neurons, we induced cLTD with NMDA and then fixed and immunolabeled cells using antibodies targeting GluA2 and the early endosome marker EEA1 0, 3, 10, and 20 min post NMDA treatment (Figures 3I–3K). GluA2 did not colocalize with EEA1 under basal conditions. However, GluA2 began to colocalize with early endosomes 3 min post NMDA treatment in control neurons and then no longer colocalized after 10 or 20 min, indicating AMPAR trafficking out of early endosomes and into recycling or late endosomes. In contrast, PAC KD neurons did not display GluA2 and EEA1 colocalization 3 min post NMDA or 10 and 20 min post

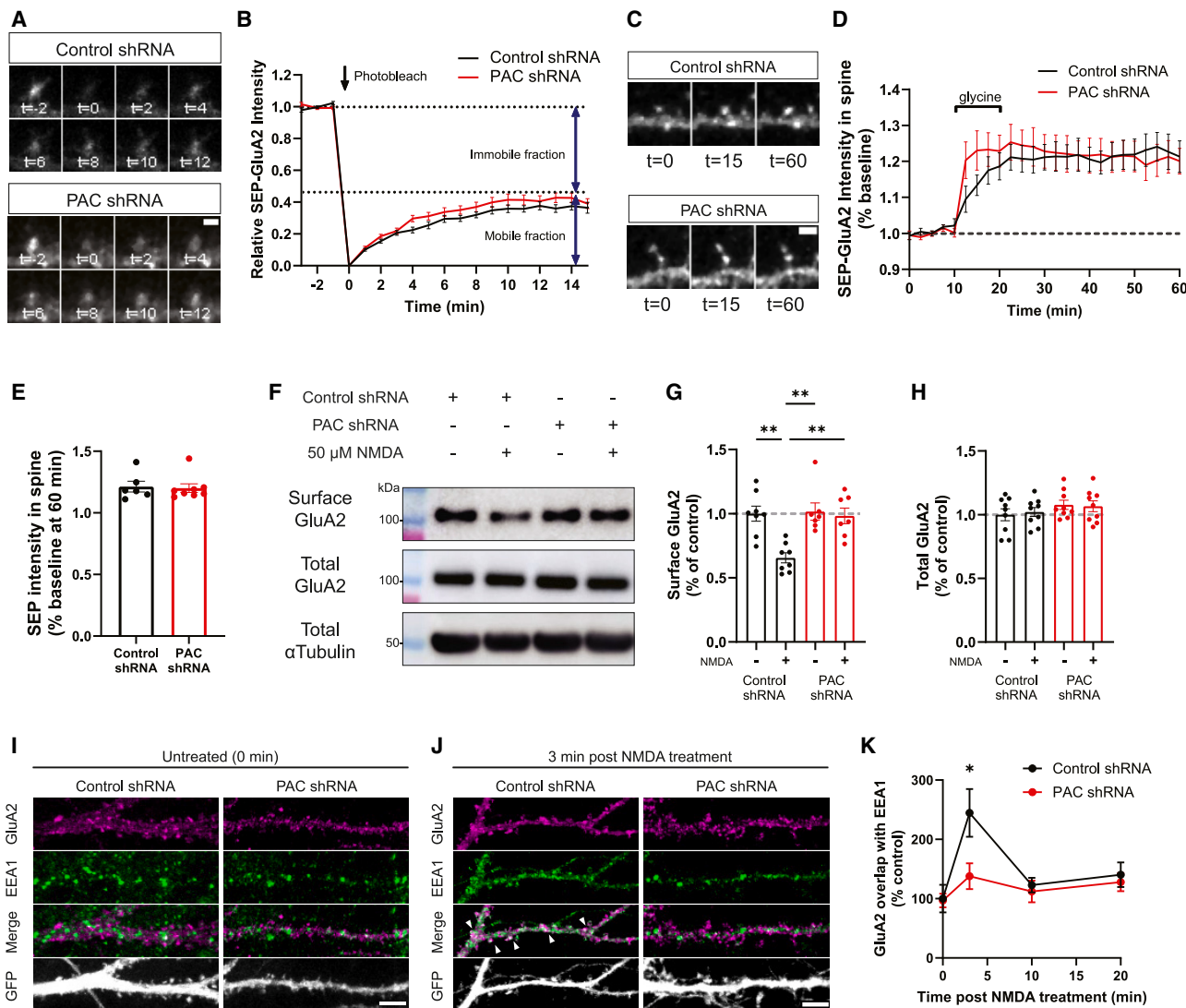


**Figure 3. PAC is required for AMPAR internalization during LTD but does not affect LTP or basal trafficking**

- (A) Representative images of SEP-GluA2 in control and PAC KD dendritic spines during photobleaching. Scale bar: 2 μm.
- (B) Quantification of FRAP of SEP-GluA2 in control ( $n = 25$ ) and PAC KD ( $n = 29$ ) neurons.
- (C) Representative images of SEP-GluA2 in control and PAC KD dendritic spines in response to glycine-induced cLTP. Scale bar: 2 μm.
- (D) Quantification of cLTP in control and PAC KD neurons over the time course of the assay.
- (E) Quantification of spine SEP intensity 60 min post-stimulation. Two-tailed Student's *t* test.
- (F) Western blot depicting surface protein levels isolated by surface biotinylation following NMDA stimulation in control and PAC KD neurons.
- (G and H) Quantification of sGluA2 and tGluA2 protein levels after cLTD and surface biotinylation.
- (I) Dendrites of unstimulated neurons showing lack of GluA2 and EEA1 colocalization in control and PAC KD neurons. Scale bar: 5 μm.
- (J) Colocalization of GluA2 and EEA1 in dendrites of control and PAC KD neurons 3 min following NMDA treatment. Scale bar: 5 μm.
- (K) Relative GluA2 intensity overlapping with EEA1 intensity 0, 3, 10, and 20 min post NMDA treatment in control ( $n = 6–14$ ) and PAC KD ( $n = 5–11$ ) neurons. Error bars represent mean ± SEM. \* $p < 0.05$ , \*\* $p < 0.01$ , two-way ANOVA with Tukey correction for multiple comparisons unless otherwise indicated.

NMDA. These results indicate that PAC KD impairs the initial trafficking of AMPARs from the cell surface to early endosomes.

AMPARs can be endocytosed through a constitutive trafficking pathway and a regulated activity-dependent pathway that have distinct molecular mechanisms.<sup>28</sup> LTD employs the activity-dependent pathway, which utilizes calcium-sensing proteins to increase AMPAR endocytosis. Homeostatic scaling is an alternative method of globally regulating surface AMPAR

levels on a longer timescale and has been reported to use the constitutive trafficking pathway. Homeostatic downscaling of AMPARs and constitutive AMPAR trafficking has been reported to use clathrin- and dynamin-independent mechanisms, whereas LTD relies on clathrin and dynamin.<sup>29,30</sup> To assess homeostatic downscaling of surface AMPARs, we employed surface biotinylation following 48 h of bicuculline treatment in neuronal cultures. We observed robust downregulation of

sGluA2 in both control and PAC KD neurons after bicuculline treatment (Figures S4A–S4C), suggesting that endocytic mechanisms involved in homeostatic scaling are not dependent on the PAC channel. Overall, we find that PAC is required for acute activity-dependent endocytosis of surface AMPAR during LTD but is not involved in mechanisms regulating constitutive trafficking or homeostatic plasticity.

#### A novel live-cell imaging cLTD assay reveals impaired AMPAR endocytosis in PAC KD neurons

In addition to biochemically probing surface AMPAR content following cLTD, we developed an imaging paradigm to detect AMPAR endocytosis in real time in live neurons. Previously, transient intracellular pH decreases following NMDA treatment quenched the fluorescence of internal SEP-AMPAR located in the dendrite endoplasmic reticulum. To circumvent this, we expressed HaloTag-GluA2 in neurons and labeled AMPARs with a cell-impermeable, pH-sensitive Halo dye, AcidifluorORANGE, which increases fluorescence intensity as pH decreases (Figure 4A). This paradigm avoids non-specific labeling of intracellular AMPARs and specifically labels surface and newly endocytosed AMPARs, which is measured through the appearance of fluorescent puncta as AcidifluorORANGE-labeled AMPARs accumulate in the acidified lumen of endosomes.

Minimal internalization is observed in untreated cells aside from normal cycling of AMPARs through the constitutive endocytic pathway. However, NMDA treatment in rat primary hippocampal neurons induces a robust increase in internalized AMPARs throughout the dendrites and soma that persists for at least 60 min and mostly undergo retrograde transport (Figure 4B; Video S1). To validate the specificity of our LTD assay, we applied D-2-amino-5-phosphonovaleric acid (D-APV), an NMDAR blocker that inhibits both LTP and LTD, to NMDA-treated neurons and found no increase in AMPAR endocytosis (Figures 4C–4E). We then measured AMPAR internalization in PAC KD neurons and PAC KD neurons expressing shRNA-resistant WT, YLAA, or K319A hPAC (Figures 4F–4H). In agreement with our surface biotinylation and fixed-cell imaging data (Figures 3F–3K), PAC KD neurons did not endocytose new AMPARs after NMDA stimulation, and endosomes remained static along dendrites (Figures 4F–4H; Video S1). This result suggests that regulation of endosomal pH by PAC is required for AMPAR endocytosis and endosome dynamics during LTD. Overexpression of WT PAC, but not the YLAA and K319A mutants, rescued AMPAR endocytosis, suggesting that, similar to pH regulation, proper PAC endosomal localization and  $\text{Cl}^-$  channel function are both required for the expression of LTD and the initial step of surface-to-early-endosome internalization of AMPARs during LTD.

#### Pyramidal neuron-specific PAC KO mice have normal dendritic spine density and basal synaptic transmission

To investigate the physiological consequences of PAC deletion in neurons, we generated a conditional PAC knockout (cKO) mouse where *Pacc1* is specifically deleted in pyramidal neurons in the hippocampus and neocortex by crossing *Pacc1* floxed mice ( $\text{PAC}^{\text{FF}}$ ) with the *NEX-Cre* line.<sup>31</sup> The PAC cKO mice were viable and grossly normal. Transcript levels of PAC in whole

hippocampal tissue were significantly reduced, with remaining transcripts likely originating from glial cells. The dendritic spine density of hippocampal CA1 pyramidal neurons in PAC cKO mice (1.076 spines/ $\mu\text{m}$ ) and littermate controls (0.9997 spines/ $\mu\text{m}$ ) was similar (Figure S5C). To test whether PAC deletion affects excitatory synaptic transmission, we prepared acute hippocampal slices and measured miniature excitatory postsynaptic currents (mEPSCs) in CA1 neurons using whole-cell electrophysiology in the presence of tetrodotoxin (TTX) to block neuronal activity (Figure S5D). The amplitude of mEPSCs, which can be attributed to post-synaptic AMPAR density or pre-synaptic vesicle loading, was similar between WT and PAC cKO mice (Figure S5E). The frequency of mEPSCs, determined by synapse number and vesicle release probability, was also comparable between WT and PAC cKO mice (Figure S5F). We then evoked CA1 EPSCs by stimulating the Schaffer collateral axons to determine how PAC deletion would affect synaptic transmission but did not observe any difference in evoked EPSC amplitude between groups (Figures S5G and S5H). Finally, we used voltage clamping to quantify CA1 AMPAR and NMDAR properties by measuring current amplitude at  $-70$  mV and  $+40$  mV, respectively. The resulting AMPA/NMDA ratio, which describes the synaptic content and strength of these receptors, was also unchanged in PAC cKO mice (Figures S5I and S5J).

*NEX-Cre* is active during embryonic development, and the effects of chronic PAC deletion on synaptic transmission may be diminished by compensatory mechanisms during neural development. To rule out this hypothesis, we acutely deleted PAC in  $\text{PAC}^{\text{FF}}$  mice by injecting the CA1 hippocampus with adeno-associated viruses (AAVs) expressing Cre-GFP or GFP alone downstream of a  $\text{Ca}^{2+}$ /calmodulin-dependent protein kinase II promoter. Acute hippocampal slices were obtained from AAV-injected mice 1 week post injection for electrophysiological recordings and morphological analysis. GFP was well expressed in hippocampal CA1 pyramidal neurons, and mEPSCs were measured in GFP-positive cells (Figure S5K). The recording pipette was filled with biocytin for post hoc analysis of dendritic spine density. Dendritic spine densities were comparable between GFP-expressing (0.9119 spines/ $\mu\text{m}$ ) and Cre-expressing neurons (0.9332 spines/ $\mu\text{m}$ ) (Figure S5L). We found that both mEPSC amplitude and frequency were also similar between GFP- and Cre-expressing neurons (Figures S5M–S5O), suggesting that acute deletion of PAC does not significantly alter neuronal morphology or synaptic transmission. Taken together, we conclude that the PAC channel is dispensable for hippocampal excitatory synaptic transmission under basal conditions.

#### PAC cKO mice have normal hippocampal LTP but impaired NMDAR-dependent and mGluR-dependent LTD

Based on our observation that PAC KD neurons have impaired activity-dependent AMPAR internalization, we tested whether synaptic plasticity was impaired in hippocampal brain slices. We measured the Schaffer collateral-evoked field excitatory postsynaptic potential (fEPSP) slope after inducing NMDA receptor-dependent LTP and LTD with theta burst stimulation (TBS) and low-frequency stimulation (LFS), respectively. Interestingly, PAC cKO CA1 hippocampus exhibited markedly

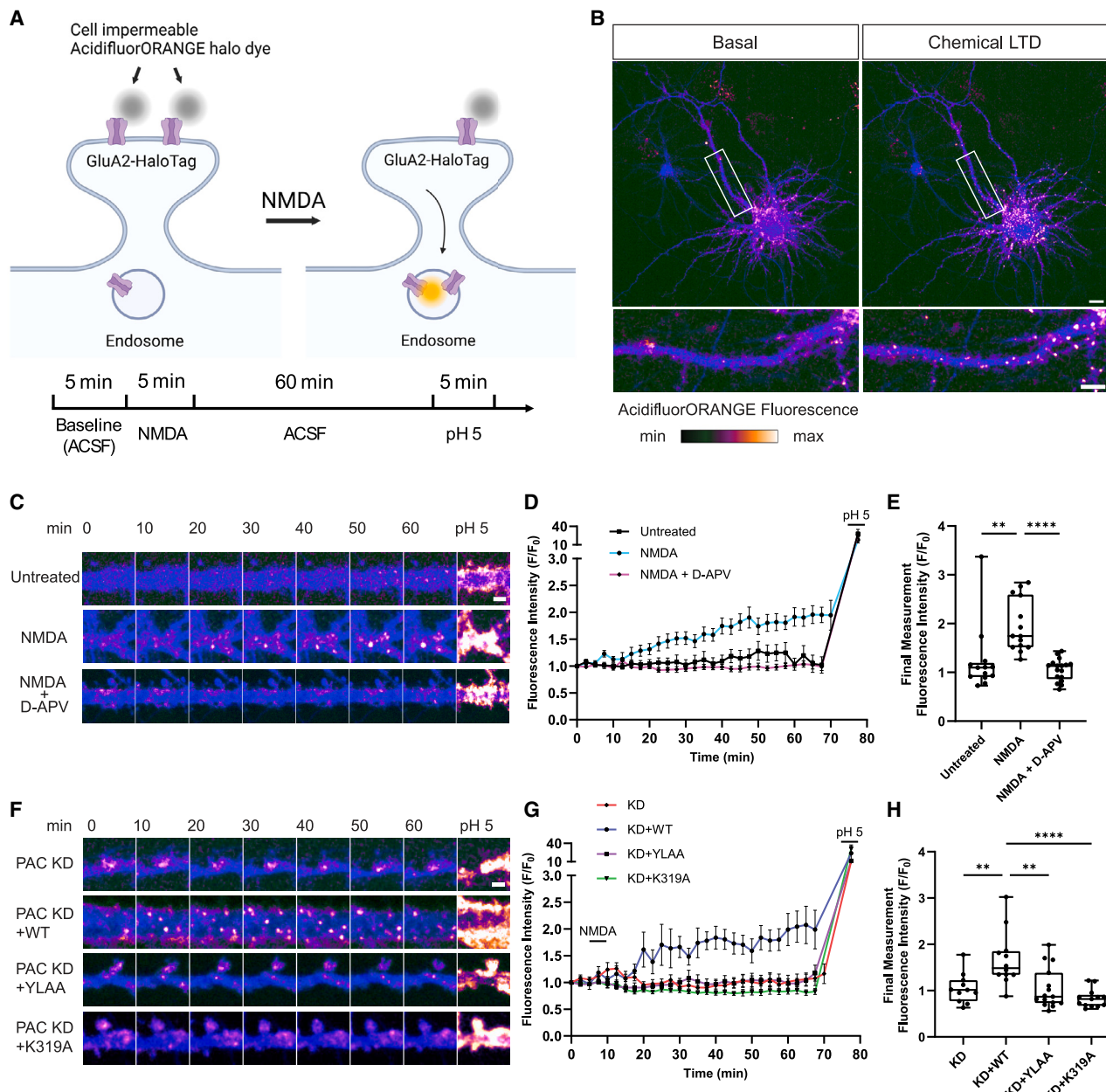


**Figure 4. Live-cell cLTD assay tracks the endocytosis of GluA2, which is impaired in PAC KD neurons**

(A) Schematic of the live-cell cLTD imaging assay. Neurons expressing Halo-GluA2 are loaded with the pH-sensitive Halo dye AcidifluorORANGE prior to induction of cLTD using NMDA.

(B) Representative neuron expressing Halo-GluA2 and GFP cell fill (blue) before and after NMDA stimulation, demonstrating the internalization of Halo-tagged AMPA receptors. Scale bars: top, 10  $\mu$ m; bottom, 5  $\mu$ m.

(C) Representative images of neurons treated with NMDA ( $n = 14$ ), left untreated ( $n = 13$ ), or treated with both NMDA and D-APV ( $n = 17$ ). Scale bar: 2  $\mu$ m. See also Video S1.

(D) Quantification of the fluorescence intensity of the AcidifluorORANGE signal during the assay.

(E) Quantification of the final versus initial fluorescence intensity for each condition.

(F) Representative images of PAC shRNA-treated neurons alone ( $n = 11$ ) or along with WT PAC cDNA ( $n = 12$ ) or the PAC mutants YLAA ( $n = 15$ ) or K319A ( $n = 13$ ). Scale bar: 2  $\mu$ m. See also Video S1.

(G) Quantification of the fluorescence intensity of the AcidifluorORANGE signal during the assay for neurons expressing PAC shRNA.

(H) Quantification of the final versus initial fluorescence intensity for each condition.

Box plots represent the interquartile range, median, minimum, and maximum values. \* $p < 0.05$ , \*\* $p < 0.01$ , \*\*\* $p < 0.001$ , \*\*\*\* $p < 0.0001$ , two-way ANOVA with Tukey correction for multiple comparisons.

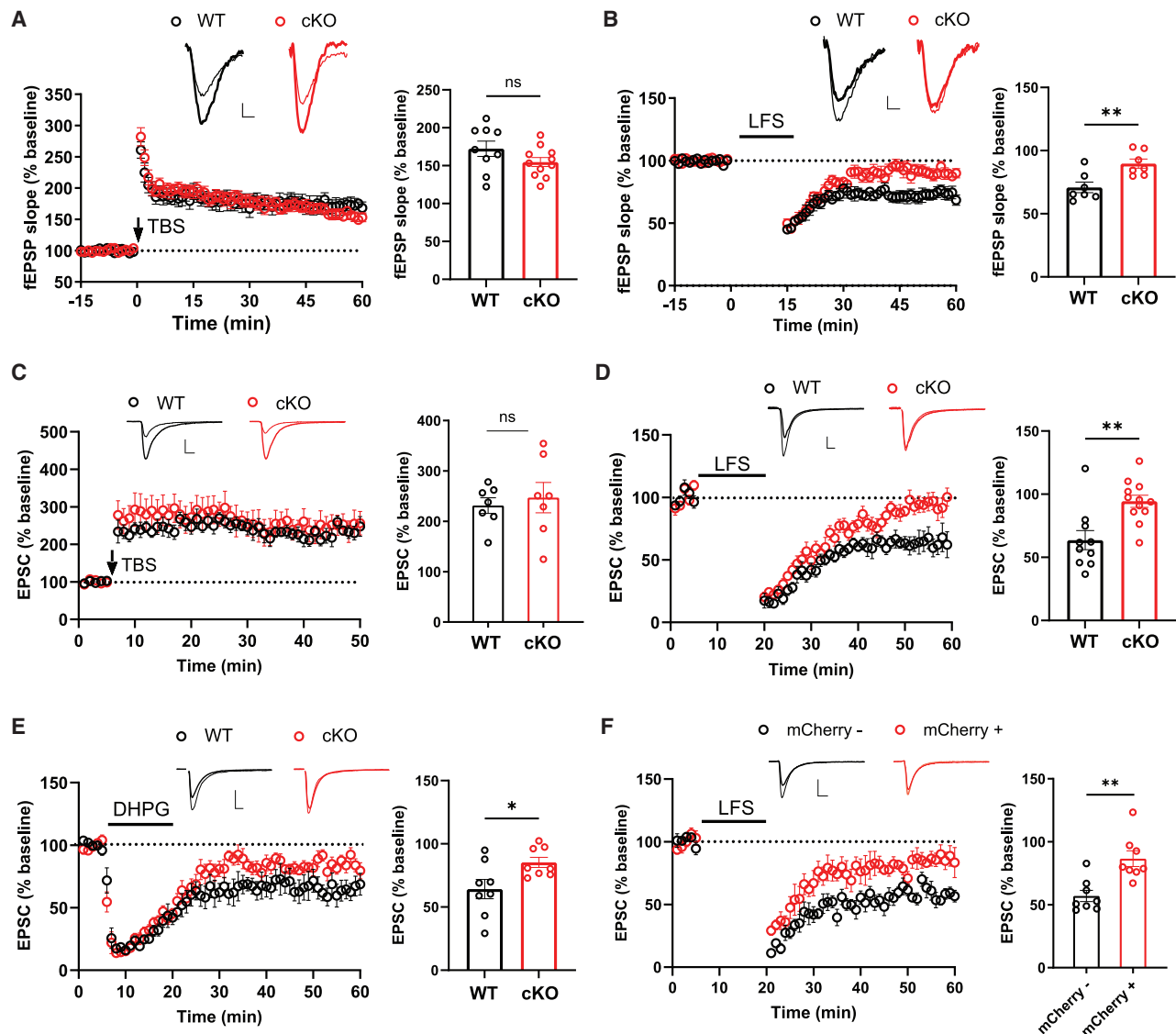


**Figure 5. PAC cKO mice have impaired NMDAR- and mGluR-dependent LTD but normal LTP**

(A) Field recordings from acute hippocampal slices: TBS-induced LTP at the Schaffer collateral-CA1 synapses with representative traces of fEPSPs taken before (thin) and 50 min after (thick) TBS stimulation. Scale bars: 0.1 mV (vertical) and 5 ms (horizontal).

(B) LFS-induced LTD at the Schaffer collateral-CA1 synapses with representative traces of fEPSPs taken before (thin) and 50 min after (thick) LFS stimulation. Scale bars: 0.1 mV (vertical) and 5 ms (horizontal). Shown are whole-cell recordings from CA1 pyramidal neurons.

(C) TBS-induced LTP in CA1 neurons with representative EPSC traces before (thin) and 50 min after (thick) TBS stimulation. Scale bars: 50 pA (vertical) and 10 ms (horizontal).

(D) LFS-induced NMDAR-dependent LTD in CA1 neurons with representative EPSC traces before (thin) and 50 min after (thick) LFS stimulation. Scale bars: 50 pA (vertical) and 10 ms (horizontal).

(E) DHPG-induced mGluR-dependent LTD in CA1 neurons with representative EPSC traces before (thin) and 50 min after (thick) LFS stimulation. Scale bars: 50 pA (vertical) and 10 ms (horizontal).

(F) LFS-induced LTD in sparsely electroporated CA1 neurons expressing hSyn-Cre-mCherry or Cre-mCherry with representative EPSC traces before (thin) and 50 min after (thick) LFS stimulation. Scale bars: 50 pA (vertical) and 10 ms (horizontal).

Quantification of fEPSP slopes or EPSCs for the final 10 min of the protocol is shown on the right. Recordings were conducted on male and female 1-2-month-old mice. Data are reported as mean  $\pm$  SEM. \*\* $p$  < 0.01, \* $p$  < 0.05. Student's t test.

impaired LTD, while LTP remained normal (Figures 5A and 5B). To examine the role of PAC in synaptic plasticity at single-cell levels, we performed whole-cell recordings in hippocampal

CA1 pyramidal neurons. Consistent with the fEPSP measurements, individual PAC cKO neurons exhibited normal LTP but impaired LTD (Figures 5C and 5D).

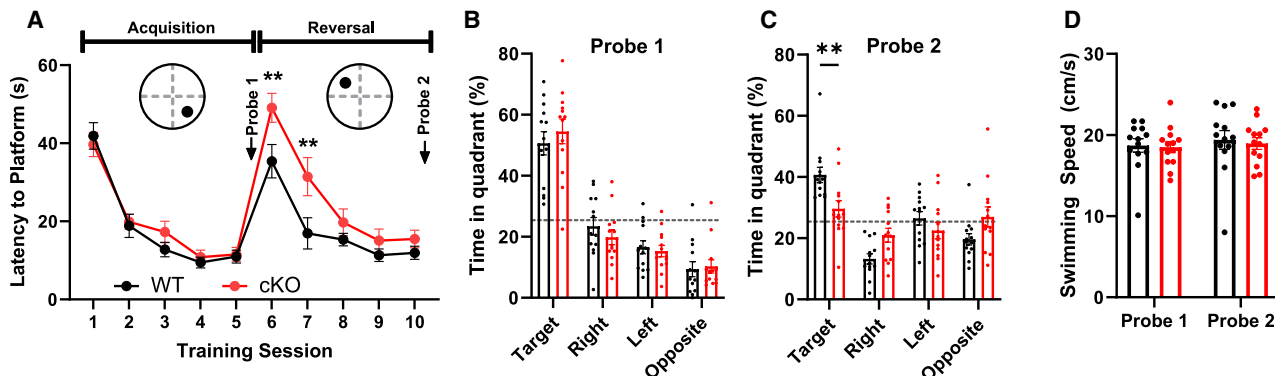


**Figure 6.** PAC cKO mice have impaired reversal learning

(A) Latency to platform during the spatial acquisition phase and the reversal phase during MWM training. Male mice aged 2–5 months were used for the behavioral assay (WT,  $n = 13$ ; cKO  $n = 13$ ).

(B) Quantification of time spent in each quadrant during probe trial 1 following acquisition training.

(C) Quantification of time spent in each quadrant during probe trial 2 following reversal training.

(D) Quantification of swim speeds for WT and cKO mice.

Data represent mean  $\pm$  SEM. \*\* $p < 0.01$ . Two-way ANOVA with Bonferroni's correction for multiple comparisons.

LTD and AMPAR internalization can also be induced by the activation of type I metabotropic glutamate receptors (mGluRs), including mGluR1 and mGluR5. mGluR-LTD has different upstream molecular signaling mechanisms than NMDAR-dependent LTD, but both forms of LTD result in AMPAR endocytosis.<sup>32</sup> To determine whether mGluR-LTD is also impaired in PAC cKO mice, we treated hippocampal slices with the type I mGluR agonist dihydroxyphenylglycine (DHPG). DHPG treatment induced robust LTD in WT but not in PAC cKO neurons (Figure 5E), indicating that AMPAR internalization may be the common mechanism impaired in PAC cKO neurons. To rule out whether mGluR-LTD is affected by surface expression of mGluRs, we used surface biotinylation to measure surface mGluR5 levels in control and PAC KD neurons and found no difference (Figure S2C).

To assess whether the LTD defect is a cell-autonomous phenotype, we sparsely expressed hSyn-Cre-mCherry in CA1 neurons from PAC<sup>F/F</sup> mice using *in utero* electroporation. EPSCs were measured from neurons from the same mouse to compare LFS-induced LTD by whole-cell recordings. Cre-mCherry-negative control neurons had robust LTD, whereas Cre-mCherry-positive neurons had impaired LTD (Figure 5F). Given the sparse transfection of the plasmid, we conclude that defects in LTD are cell autonomous and are likely caused by impaired AMPAR endocytosis rather than changes in presynaptic release. Based on our results from recording neural activity in hippocampal brain slices, we conclude that the regulation of endosomal pH through PAC is required for NMDAR- and mGluR-dependent LTD in the hippocampus but is not essential for LTP.

#### PAC cKO mice have impaired reversal learning

Impairments in synaptic plasticity often manifest in cognitive and behavioral deficits. We conducted a battery of behavioral tests in male PAC cKO mice alongside WT littermate controls to assess cognitive and behavioral function. PAC cKO mice displayed normal locomotion during 30 min of testing in the open field

test (Figure S7A). Anxiety, measured in the elevated plus maze, was comparable between WT and cKO mice (Figure S7B). We next performed behavioral assays that require functional LTP, including the Y maze, contextual fear conditioning, and the Morris water maze (MWM). Since hippocampal LTP appears normal in PAC cKO mice, we added an additional reversal training session and probe to the MWM assay to assess LTD. As expected, assays dependent on hippocampal LTP, including the spontaneous alternation in the Y maze (Figure S7C), contextual fear memory following fear conditioning (Figures S7D–S7F), and MWM spatial acquisition (Figures 6A and 6B), were all normal in PAC cKO mice. The MWM reversal task is dependent on hippocampal LTD for behavioral flexibility, or the ability to appropriately adapt to a changing environment.<sup>10,33</sup> Interestingly, cKO mice performed worse in the reversal task during the first 2 days of reversal training (Figure 6A). PAC cKO mice also performed worse than WT mice during probe trial 2 (Figure 6C), spending reduced time in the correct target quadrant. Swimming speeds were comparable between WT and cKO mice (Figure 6D). Altogether, our behavioral results are consistent with our *in vitro* and *ex vivo* data, demonstrating that PAC deletion in pyramidal neurons impairs LTD, while basal synaptic transmission and LTP are maintained. This is reflected in the behavior of PAC cKO mice, where otherwise normally performing mice have impaired behavioral flexibility.

#### DISCUSSION

In this study, we revealed a prominent role of the PAC channel and endosomal hyper-acidification in regulating activity-dependent AMPAR internalization and LTD in hippocampal neurons. PAC-deficient neurons have markedly lower endosomal pH and impaired LTD due to a defect in AMPAR endocytosis. Consequently, neuronal PAC deletion in mice impairs adaptive behavior. While both LTP and LTD are important for synaptic plasticity, the molecular tools to study LTD are less developed

than those for LTP, and many inhibitors of LTD also affect LTP.<sup>32</sup> Thus, we utilized HaloTag-GluA2 to track AMPAR endocytosis in live neurons. LTD is essential for cognitive functions such as memory, behavioral flexibility, and novelty detection. Furthermore, dysregulation of synaptic plasticity is implicated in neurodegenerative diseases such as Alzheimer's disease (AD), where aberrant cellular signaling may cause pathological synaptic depression and loss.<sup>34</sup> Defects in endosomal acid-base regulation have also been implicated in AD.<sup>35</sup> Our study provides further evidence of the importance of pH regulation by introducing PAC as a novel player. Additionally, targeting PAC to restore endosomal function may offer a potential therapeutic strategy for mitigating deficits in synaptic plasticity in degenerative diseases.

It is well established that proper pH or Cl<sup>-</sup> regulation within the endolysosomal system is crucial for neural development and synaptic function, as evidenced by studies on the endosomal sodium proton exchangers NHE6 and NHE9<sup>35</sup> or the chloride transporters CLC-3<sup>36</sup> and CLC-4.<sup>37</sup> Loss of function of NHE6/9 results in hyper-acidified endosomes and has diverse outcomes, including impaired neurite development,<sup>15</sup> dendritic spine density,<sup>38</sup> endolysosomal maturation,<sup>16</sup> and synaptic transmission.<sup>14</sup> Similarly, endosome alkalinization also results in impaired neural phenotypes, most notably abolishing LTD and AMPAR endocytosis in the cerebellum<sup>7</sup> and disrupting dendritic branching and cargo uptake.<sup>39</sup> We demonstrate that neuronal PAC functions as an early and recycling endosome channel that regulates luminal pH, which is consistent with other reports describing the subcellular localization of PAC and its role in preventing luminal hyper-acidification.<sup>18,19</sup> While PAC is also present on the plasma membrane, our data indicate that the main function of PAC is endosomal. Based on our localization and electrophysiology data, it is unlikely that PAC regulates pre-synaptic plasticity. Interestingly, the consequences of PAC deletion are less severe compared to the deletions of NHE6, NHE9, or CLC-3, which cause broad neurodevelopmental defects. Instead, PAC is directly involved in LTD by facilitating the rapid removal of AMPARs from the synapse through endocytosis. Thus, cellular changes brought about by loss of NHEs or CLCs are not as well tolerated compared to loss of PAC. How PAC differs from other endosomal ion transporters in regulating neural function remains to be determined.

To directly observe AMPAR endocytosis in live neurons, we developed a cLTD assay utilizing HaloTag-GluA2 and the AcidifluorORANGE Halo dye. This assay addresses a known limitation of SEP-tagged AMPARs, where NMDA causes non-specific fluorescence quenching of intracellular SEP-AMPARs located in the endoplasmic reticulum.<sup>27</sup> Using HaloTag-GluA2 provides several advantages. First, using a variety of Halo dyes with different properties allows for temporal control over AMPAR labeling. Newly endocytosed AMPARs can be measured by using a membrane-impermeable dye that becomes fluorescent in the low-pH environment of the endosome. Second, this method allows for the longitudinal tracking of endocytosed AMPARs in neurons over the whole period of LTD induction, allowing the direct visualization of endocytic events, endosomal maturation and fusion, and anterograde or retrograde trafficking, which have not been observed previously. In un-

treated neurons, our assay reveals both endocytic and exocytic events, though there is rarely a net increase in endocytosed AMPARs over time. During cLTD, we observed robust AMPAR endocytosis, maturation, and retrograde transport, which were absent in PAC KD neurons. Interestingly, a recent study has shown pH dependence of organelle processivity using genetic manipulation of NHE9 to alter luminal acidification.<sup>40</sup> Measuring receptor trafficking dynamics with our cLTD assay may prove valuable for future studies investigating the mechanisms underlying the complex cellular trafficking events of AMPARs and can be adapted for *in vivo* experiments.

The role of endosomal pH in synaptic plasticity is largely unexplored. Aside from a recent study showing that optogenetic alkalinization of endosomes impairs LTD and AMPAR endocytosis in the cerebellum,<sup>7</sup> there is little direct evidence linking altered luminal pH to AMPAR trafficking. In contrast to alkalinization, we used PAC deletion to hyper-acidify endosomes and observed a similar LTD defect in hippocampal neurons. In PAC-deficient neurons, this LTD defect is brought about by ineffective delivery of AMPARs from the plasma membrane to the early endosome through an unknown mechanism. We speculate that altered endosome pH may disrupt protein-protein interactions between AMPARs and trafficking machinery that are necessary for clathrin-mediated endocytosis of AMPARs, including TARPγ2 (Stargazin), PICK1, GRIP1, or BRAG2. Future studies are necessary to reveal the exact players in LTD that are involved when pH homeostasis is disrupted.

Despite robust impairment of LTD, we found no such impairment in LTP or basal synaptic transmission in PAC-null neurons. Similar patterns of impaired LTD but normal LTP have been reported in studies of mice lacking the calcium-sensitive proteins PICK1,<sup>8,41</sup> which is involved in the endocytosis and retention of GluA2, and synaptotagmin-3,<sup>10</sup> which is crucial for the activity-dependent endocytosis of GluA2. Optogenetic alkalinization also does not alter LTP or basal synaptic transmission.<sup>7</sup> These results collectively support a model where LTP is less reliant on endocytic machinery for the early stages of AMPAR delivery to the PSD. Indeed, the lateral diffusion of AMPARs is a major contributor to receptor enrichment at dendritic spines during LTP.<sup>3</sup> Our data support this model, but it remains possible that impaired endosomal acidification may be involved in later stages of LTP, where AMPARs need to be exocytosed from intracellular stores to replenish membrane AMPAR levels.<sup>42</sup>

Endosomal hyper-acidification resulting from PAC deletion does not appear to alter surface expression of many proteins, including AMPARs, and does not affect basal synaptic transmission. Mechanisms regulating AMPAR endocytosis are context dependent and use distinct molecular pathways. Endocytosis can occur through a constitutive trafficking pathway that maintains surface AMPAR content or an activity-dependent regulated pathway that reduces surface AMPAR levels.<sup>28–30</sup> The regulated pathway involves the specific removal of GluA2-containing AMPARs from the membrane following PKC phosphorylation at the S880 residue.<sup>2,43</sup> GluA2 first dissociates from the PSD and diffuses to endocytic zones. Endocytosis occurs either through direct binding to the AP-2 adaptor complex or via AMPAR-interacting proteins that deliver AMPARs to the endocytic machinery.<sup>44</sup> In contrast, slower endocytic events, such

as constitutive trafficking and homeostatic downscaling, utilize an Arf6-dependent clathrin-independent pathway.<sup>30</sup> We hypothesize that proteins involved in these distinct pathways rely differently on the pH of the endosome and PAC channel function. Alternatively, compensatory mechanisms in PAC-deficient neurons may account for the normal surface expression of AMPARs but may not be effective during acute neuronal activity such as LTD.

Interestingly, we have found previously that PAC deletion in HEK293 cells modestly increased the surface expression of TfRs and transferrin uptake, but this was not observed in neurons. The difference in energy and nutrient requirements between cancer cell lines and post-mitotic cultured neurons may account for this discrepancy. Additionally, TfR and AMPAR constitutive trafficking utilize different pathways in neurons and may undergo differential regulation. Regardless, there could be cell-type-specific roles of PAC that remain to be explored. Based on our data and the existing literature, we conclude that PAC and endosomal acidification are required only for rapid, activity-dependent AMPAR endocytosis, whereas the constitutive pathway appears to be less sensitive to perturbations in endosomal pH.

We showed that PAC is important for endosomal pH balance and LTD in neurons. However, the molecular players involved in linking endosomal pH to LTD remain elusive due to redundancy in endocytic machinery. Nevertheless, the discovery that endosomal hyper-acidification ablates hippocampal LTD serves as a counterpart to the previous finding that endosomal alkalinization impairs LTD in the cerebellum and has broader implications in neurobiology. Currently, it is unknown whether the LTD impairments caused by hyper-acidification and alkalinization of the endosome result from the same or distinct mechanisms. It would be important to test whether trafficking of other neurotransmitter receptors is similarly affected by altered endosomal acidification. Additionally, exploring whether PAC is involved in LTD and AMPAR trafficking in Purkinje cells of the cerebellum, and its impact on motor learning, could provide further insights. Dysregulation of endosome function is also implicated in autism and AD, but it remains unclear whether PAC contributes to the pathogenesis of these disorders. As proper LTD and endosomal function is important for synaptic function throughout the CNS, it is likely that future studies will uncover novel roles of PAC in different physiological and pathological contexts.

### Limitations of the study

We reported the importance of PAC in regulating synaptic LTD and animal behavior; however, there are several caveats of the work to address. One limitation is that we measured AMPAR dynamics *in vitro* in neurons overexpressing GluA2. Now, with the development of SEP-GluA2 and HaloTag-GluA2 transgenic mice, these experiments can be repeated with endogenous proteins and potentially *ex vivo* or *in vivo* with two-photon imaging. The dynamics of different AMPAR subunits, especially GluA1, can also be measured with these endogenous AMPAR expression models.

We report the use of HaloTag-GluA2 as a suitable experimental paradigm to observe AMPAR endocytosis and trafficking during cLTD. There are several limitations to this method due to

the pH dependence of the AcidifluorORANGE dye. First, early endocytic events prior to endosomal acidification and maturation are not observable with this technique. Second, the identity of acidified vesicles is unknown using this technique but would provide valuable insight into the trafficking dynamics of AMPARs.

### RESOURCE AVAILABILITY

#### Lead contact

Requests for further information and resources should be directed to and will be fulfilled by the lead contact, Zhaozhu Qiu ([zhaozhu@jhmi.edu](mailto:zhaozhu@jhmi.edu)).

#### Materials availability

All unique/stable reagents generated in this study are available from the [lead contact](#) with a completed materials transfer agreement. Plasmids generated during this study were deposited on Addgene.

#### Data and code availability

- Any additional data are available from the [lead contact](#) upon request.
- No new code was generated for this study.
- Any additional information required to analyze the data is available from the [lead contact](#) upon request.

### ACKNOWLEDGMENTS

The authors thank Seth Margolis for insightful discussion and Andrew Holland for providing microscope access. This work was supported by grants from the National Institutes of Health (NIH R01NS118014, R35GM124824, and RF1NS134549 to Z.Q. and R37NS036715 to R.L.H.). Z.Q. was also supported by the American Heart Association (AHA) Established Investigator Award, McKnight Scholar Award, Klingenstein-Simon Scholar Award, Sloan Research Fellowship in Neuroscience, and Randall Reed Scholar Award. Research reported in this publication was supported by the Office of the Director of the NIH under award S10OD034393 to Scot Kuo for use of the Johns Hopkins Microscope Facility. J.Y. was supported by AHA postdoctoral fellowship 20POST35200185 and Career Development Award 857671. BioRender was used to generate several figures.

### AUTHOR CONTRIBUTIONS

K.H.C. designed and performed the majority of experiments. K.H.C. and Z.Q. designed the study and wrote the manuscript with input from all authors. J.Y., C.J., and N.K. performed electrophysiological recordings. K.H.C. and B.L. performed and developed live-neuron imaging assays under the supervision of R.H. Z.Z. and S.S. provided critical reagents.

### DECLARATION OF INTERESTS

The authors declare no competing interests.

### STAR★METHODS

Detailed methods are provided in the online version of this paper and include the following:

- [KEY RESOURCES TABLE](#)
- [EXPERIMENTAL MODEL AND SUBJECT DETAILS](#)
  - Animals
  - Primary neuron cultures and transfection
  - Human iPSC-derived neurons
- [METHOD DETAILS](#)
  - Lentivirus production and transduction
  - Immunocytochemistry
  - Live-cell imaging for endosomal pH

- Live-cell imaging of SEP-GluA2 for AMPAR trafficking and chemical LTD
- Live-cell imaging of HaloTag-GluA2 for chemical LTD
- Chemical LTD and surface biotinylation
- Stereotactic surgeries
- In-utero electroporation
- Electrophysiological recordings
- Behavioral analysis

● QUANTIFICATION AND STATISTICAL ANALYSIS

SUPPLEMENTAL INFORMATION

Supplemental information can be found online at <https://doi.org/10.1016/j.celrep.2025.115302>.

Received: September 10, 2024

Revised: December 16, 2024

Accepted: January 23, 2025

Published: February 12, 2025

REFERENCES

1. Magee, J.C., and Grienberger, C. (2020). Synaptic Plasticity Forms and Functions. *Annu. Rev. Neurosci.* 43, 95–117. <https://doi.org/10.1146/annurev-neuro-090919-022842>.
2. Diering, G.H., and Huganir, R.L. (2018). The AMPA Receptor Code of Synaptic Plasticity. *Neuron* 100, 314–329. <https://doi.org/10.1016/j.neuron.2018.10.018>.
3. Borgdorff, A.J., and Choquet, D. (2002). Regulation of AMPA receptor lateral movements. *Nature* 417, 649–653. <https://doi.org/10.1038/nature00780>.
4. Ehlers, M.D. (2000). Reinsertion or degradation of AMPA receptors determined by activity-dependent endocytic sorting. *Neuron* 28, 511–525. [https://doi.org/10.1016/s0896-6273\(00\)00129-x](https://doi.org/10.1016/s0896-6273(00)00129-x).
5. Matsuda, S., Kakegawa, W., Budisantoso, T., Nomura, T., Kohda, K., and Yuzaki, M. (2013). Stargazin regulates AMPA receptor trafficking through adaptor protein complexes during long-term depression. *Nat. Commun.* 4, 2759. <https://doi.org/10.1038/ncomms3759>.
6. Citri, A., and Malenka, R.C. (2008). Synaptic plasticity: multiple forms, functions, and mechanisms. *Neuropsychopharmacology* 33, 18–41. <https://doi.org/10.1038/sj.npp.1301559>.
7. Kakegawa, W., Katoh, A., Narumi, S., Miura, E., Motohashi, J., Takahashi, A., Kohda, K., Fukazawa, Y., Yuzaki, M., and Matsuda, S. (2018). Optogenetic Control of Synaptic AMPA Receptor Endocytosis Reveals Roles of LTD in Motor Learning. *Neuron* 99, 985–998.e6. <https://doi.org/10.1016/j.neuron.2018.07.034>.
8. Lin, D.T., and Huganir, R.L. (2007). PICK1 and phosphorylation of the glutamate receptor 2 (GluR2) AMPA receptor subunit regulates GluR2 recycling after NMDA receptor-induced internalization. *J. Neurosci.* 27, 13903–13908. <https://doi.org/10.1523/JNEUROSCI.1750-07.2007>.
9. Xia, J., Zhang, X., Staudinger, J., and Huganir, R.L. (1999). Clustering of AMPA receptors by the synaptic PDZ domain-containing protein PICK1. *Neuron* 22, 179–187. [https://doi.org/10.1016/s0896-6273\(00\)80689-3](https://doi.org/10.1016/s0896-6273(00)80689-3).
10. Awasthi, A., Ramachandran, B., Ahmed, S., Benito, E., Shinoda, Y., Nitzzan, N., Heukamp, A., Rannio, S., Martens, H., Barth, J., et al. (2019). Synaptotagmin-3 drives AMPA receptor endocytosis, depression of synapse strength, and forgetting. *Science* 363, eaav1483. <https://doi.org/10.1126/science.aav1483>.
11. Chiu, S.L., Diering, G.H., Ye, B., Takamiya, K., Chen, C.M., Jiang, Y., Nir-anjan, T., Schwartz, C.E., Wang, T., and Huganir, R.L. (2017). GRASP1 Regulates Synaptic Plasticity and Learning through Endosomal Recycling of AMPA Receptors. *Neuron* 93, 1405–1419.e8. <https://doi.org/10.1016/j.neuron.2017.02.031>.
12. Brown, T.C., Tran, I.C., Backos, D.S., and Esteban, J.A. (2005). NMDA receptor-dependent activation of the small GTPase Rab5 drives the removal of synaptic AMPA receptors during hippocampal LTD. *Neuron* 45, 81–94. <https://doi.org/10.1016/j.neuron.2004.12.023>.
13. Fernández-Monreal, M., Brown, T.C., Royo, M., and Esteban, J.A. (2012). The balance between receptor recycling and trafficking toward lysosomes determines synaptic strength during long-term depression. *J. Neurosci.* 32, 13200–13205. <https://doi.org/10.1523/JNEUROSCI.0061-12.2012>.
14. Ullman, J.C., Yang, J., Sullivan, M., Bendor, J., Levy, J., Pham, E., Silm, K., Seifkar, H., Sohal, V.S., Nicoll, R.A., and Edwards, R.H. (2018). A mouse model of autism implicates endosome pH in the regulation of presynaptic calcium entry. *Nat. Commun.* 9, 330. <https://doi.org/10.1038/s41467-017-02716-5>.
15. Ouyang, Q., Lizarraga, S.B., Schmidt, M., Yang, U., Gong, J., Ellisor, D., Kauer, J.A., and Morrow, E.M. (2013). Christianson syndrome protein NHE6 modulates TrkB endosomal signaling required for neuronal circuit development. *Neuron* 80, 97–112. <https://doi.org/10.1016/j.neuron.2013.07.043>.
16. Pescosolido, M.F., Ouyang, Q., Liu, J.S., and Morrow, E.M. (2021). Loss of Christianson syndrome Na+/H+ exchanger 6 (NHE6) causes abnormal endosome maturation and trafficking underlying lysosome dysfunction in neurons. *J. Neurosci.* 41, 9235–9256. <https://doi.org/10.1523/JNEUROSCI.1244-20.2021>.
17. Yang, J., Chen, J., Del Carmen Vitery, M., Osei-Owusu, J., Chu, J., Yu, H., Sun, S., and Qiu, Z. (2019). PAC, an evolutionarily conserved membrane protein, is a proton-activated chloride channel. *Science* 364, 395–399. <https://doi.org/10.1126/science.aav9739>.
18. Osei-Owusu, J., Yang, J., Leung, K.H., Ruan, Z., Lü, W., Krishnan, Y., and Qiu, Z. (2021). Proton-activated chloride channel PAC regulates endosomal acidification and transferrin receptor-mediated endocytosis. *Cell Rep.* 34, 108683. <https://doi.org/10.1016/j.celrep.2020.108683>.
19. Zeziula, M., Blin, S., Schmitt, F.W., Lehmann, M., and Jentsch, T.J. (2022). Proton-gated anion transport governs macropinosome shrinkage. *Nat. Cell Biol.* 24, 885–895. <https://doi.org/10.1038/s41556-022-00912-0>.
20. Ullrich, F., Blin, S., Lazarow, K., Daubitz, T., von Kries, J.P., and Jentsch, T.J. (2019). Identification of TMEM206 proteins as pore of PAORAC/ASOR acid-sensitive chloride channels. *Elife* 8, e49187. <https://doi.org/10.7554/elife.49187>.
21. Osei-Owusu, J., Kots, E., Ruan, Z., Mihaljević, L., Chen, K.H., Tamhaney, A., Ye, X., Lü, W., Weinstein, H., and Qiu, Z. (2022). Molecular determinants of pH sensing in the proton-activated chloride channel. *Proc. Natl. Acad. Sci. USA* 119, e2200727119. <https://doi.org/10.1073/pnas.2200727119>.
22. Ruan, Z., Osei-Owusu, J., Du, J., Qiu, Z., and Lü, W. (2020). Structures and pH-sensing mechanism of the proton-activated chloride channel. *Nature* 588, 350–354. <https://doi.org/10.1038/s41586-020-2875-7>.
23. Blanpied, T.A., Scott, D.B., and Ehlers, M.D. (2002). Dynamics and regulation of clathrin coats at specialized endocytic zones of dendrites and spines. *Neuron* 36, 435–449. [https://doi.org/10.1016/s0896-6273\(02\)00979-0](https://doi.org/10.1016/s0896-6273(02)00979-0).
24. Osei-Owusu, J., Yang, J., Del Carmen Vitery, M., Tian, M., and Qiu, Z. (2020). PAC proton-activated chloride channel contributes to acid-induced cell death in primary rat cortical neurons. *Channels* 14, 53–58. <https://doi.org/10.1080/19336950.2020.1730019>.
25. Mahon, M.J. (2011). pHluorin2: an enhanced, ratiometric, pH-sensitive green fluorescent protein. *Adv. Biosci. Biotechnol.* 2, 132–137. <https://doi.org/10.4236/abb.2011.23021>.
26. Fang, H., Bygrave, A.M., Roth, R.H., Johnson, R.C., and Huganir, R.L. (2021). An optimized CRISPR/Cas9 approach for precise genome editing in neurons. *Elife* 10, e65202. <https://doi.org/10.7554/elife.65202>.
27. Rathje, M., Fang, H., Bachman, J.L., Anggono, V., Gether, U., Huganir, R.L., and Madsen, K.L. (2013). AMPA receptor pHluorin-GluA2 reports NMDA receptor-induced intracellular acidification in hippocampal

- neurons. *Proc. Natl. Acad. Sci. USA* 110, 14426–14431. <https://doi.org/10.1073/pnas.1312982110>.
28. Man, H.Y., Lin, J.W., Ju, W.H., Ahmadian, G., Liu, L., Becker, L.E., Sheng, M., and Wang, Y.T. (2000). Regulation of AMPA receptor-mediated synaptic transmission by clathrin-dependent receptor internalization. *Neuron* 25, 649–662. [https://doi.org/10.1016/s0896-6273\(00\)81067-3](https://doi.org/10.1016/s0896-6273(00)81067-3).
  29. Zheng, N., Jeyifous, O., Munro, C., Montgomery, J.M., and Green, W.N. (2015). Synaptic activity regulates AMPA receptor trafficking through different recycling pathways. *Elife* 4, e06878. <https://doi.org/10.7554/eLife.06878>.
  30. Glebov, O.O., Tigaret, C.M., Mellor, J.R., and Henley, J.M. (2015). Clathrin-independent trafficking of AMPA receptors. *J. Neurosci.* 35, 4830–4836. <https://doi.org/10.1523/JNEUROSCI.3571-14.2015>.
  31. Goebels, S., Bormuth, I., Bode, U., Hermanson, O., Schwab, M.H., and Nave, K.A. (2006). Genetic targeting of principal neurons in neocortex and hippocampus of NEX-Cre mice. *Genesis* 44, 611–621. <https://doi.org/10.1002/dvg.20256>.
  32. Collingridge, G.L., Peineau, S., Howland, J.G., and Wang, Y.T. (2010). Long-term depression in the CNS. *Nat. Rev. Neurosci.* 11, 459–473. <https://doi.org/10.1038/nrn2867>.
  33. Nicholls, R.E., Alarcon, J.M., Malleret, G., Carroll, R.C., Grody, M., Vronskaya, S., and Kandel, E.R. (2008). Transgenic mice lacking NMDAR-dependent LTD exhibit deficits in behavioral flexibility. *Neuron* 58, 104–117. <https://doi.org/10.1016/j.neuron.2008.01.039>.
  34. Li, Z., Jo, J., Jia, J.M., Lo, S.C., Whitcomb, D.J., Jiao, S., Cho, K., and Sheng, M. (2010). Caspase-3 activation via mitochondria is required for long-term depression and AMPA receptor internalization. *Cell* 141, 859–871. <https://doi.org/10.1016/j.cell.2010.03.053>.
  35. Prasad, H., and Rao, R. (2023). Endosomal Acid-Base Homeostasis in Neurodegenerative Diseases. *Rev. Physiol. Biochem. Pharmacol.* 185, 195–231. [https://doi.org/10.1007/112\\_2020\\_25](https://doi.org/10.1007/112_2020_25).
  36. Stobrawa, S.M., Breiderhoff, T., Takamori, S., Engel, D., Schweizer, M., Zdebik, A.A., Bösl, M.R., Ruether, K., Jahn, H., Draguhn, A., et al. (2001). Disruption of CIC-3, a chloride channel expressed on synaptic vesicles, leads to a loss of the hippocampus. *Neuron* 29, 185–196. [https://doi.org/10.1016/s0896-6273\(01\)00189-1](https://doi.org/10.1016/s0896-6273(01)00189-1).
  37. Guzman, R.E., Sierra-Marquez, J., Bungert-Plümke, S., Franzen, A., and Fahlke, C. (2022). Functional characterization of CLCN4 variants associated with X-linked intellectual disability and epilepsy. *Front. Mol. Neurosci.* 15, 872407. <https://doi.org/10.3389/fmol.2022.872407>.
  38. Gao, A.Y.L., Ilie, A., Chang, P.K.Y., Orlowski, J., and McKinney, R.A. (2019). A Christianson syndrome-linked deletion mutation ( $\Delta 287ES288$ ) in SLC9A6 impairs hippocampal neuronal plasticity. *Neurobiol. Dis.* 130, 104490. <https://doi.org/10.1016/j.nbd.2019.104490>.
  39. Ilie, A., Gao, A.Y.L., Boucher, A., Park, J., Berghuis, A.M., Hoffer, M.J.V., Hilhorst-Hofstee, Y., McKinney, R.A., and Orlowski, J. (2019). A potential gain-of-function variant of SLC9A6 leads to endosomal alkalinization and neuronal atrophy associated with Christianson Syndrome. *Neurobiol. Dis.* 121, 187–204. <https://doi.org/10.1016/j.nbd.2018.10.002>.
  40. Tripathy, S.K., Shamroukh, H.S., Fares, P., Bezh, Z., Akhtar, M., and Kondapalli, K.C. (2023). Acidification of the phagosome orchestrates the motor forces directing its transport. *Biochem. Biophys. Res. Commun.* 689, 149236. <https://doi.org/10.1016/j.bbrc.2023.149236>.
  41. Anggono, V., Koç-Schmitz, Y., Widagdo, J., Kormann, J., Quan, A., Chen, C.M., Robinson, P.J., Choi, S.Y., Linden, D.J., Piemann, M., and Huganir, R.L. (2013). PICK1 interacts with PACSIN to regulate AMPA receptor internalization and cerebellar long-term depression. *Proc. Natl. Acad. Sci. USA* 110, 13976–13981. <https://doi.org/10.1073/pnas.1312467110>.
  42. Park, M., Penick, E.C., Edwards, J.G., Kauer, J.A., and Ehlers, M.D. (2004). Recycling endosomes supply AMPA receptors for LTP. *Science* 305, 1972–1975. <https://doi.org/10.1126/science.1102026>.
  43. Henley, J.M., and Wilkinson, K.A. (2013). AMPA receptor trafficking and the mechanisms underlying synaptic plasticity and cognitive aging. *Dialogues Clin. Neurosci.* 15, 11–27. <https://doi.org/10.31887/DCNS.2013.15.1/jhenley>.
  44. Kastning, K., Kukhtina, V., Kittler, J.T., Chen, G., Pechstein, A., Enders, S., Lee, S.H., Sheng, M., Yan, Z., and Haucke, V. (2007). Molecular determinants for the interaction between AMPA receptors and the clathrin adaptor complex AP-2. *Proc. Natl. Acad. Sci. USA* 104, 2991–2996. <https://doi.org/10.1073/pnas.0611170104>.
  45. Yang, J., Vitery, M.D.C., Chen, J., Osei-Owusu, J., Chu, J., and Qiu, Z. (2019). Glutamate-Releasing SWELL1 Channel in Astrocytes Modulates Synaptic Transmission and Promotes Brain Damage in Stroke. *Neuron* 102, 813–827.e6. <https://doi.org/10.1016/j.neuron.2019.03.029>.
  46. Fernandopulle, M.S., Prestil, R., Grunseich, C., Wang, C., Gan, L., and Ward, M.E. (2018). Transcription Factor-Mediated Differentiation of Human iPSCs into Neurons. *Curr. Protoc. Cell Biol.* 79, e51. <https://doi.org/10.1002/cpcb.51>.
  47. Pohlkamp, T., Xian, X., Wong, C.H., Durakoglugil, M.S., Werthmann, G.C., Saido, T.C., Evers, B.M., White, C.L., Connor, J., Hammer, R.E., and Herz, J. (2021). NHE6 depletion corrects ApoE4-mediated synaptic impairments and reduces amyloid plaque load. *Elife* 10, e72034. <https://doi.org/10.7554/elife.72034>.
  48. Tan, H.L., Chiu, S.L., Zhu, Q., and Huganir, R.L. (2020). GRIP1 regulates synaptic plasticity and learning and memory. *Proc. Natl. Acad. Sci. USA* 117, 25085–25091. <https://doi.org/10.1073/pnas.2014827117>.
  49. Tan, H.L., Queenan, B.N., and Huganir, R.L. (2015). GRIP1 is required for homeostatic regulation of AMPAR trafficking. *Proc. Natl. Acad. Sci. USA* 112, 10026–10031. <https://doi.org/10.1073/pnas.1512786112>.
  50. Graves, A.R., Roth, R.H., Tan, H.L., Zhu, Q., Bygrave, A.M., Lopez-Ortega, E., Hong, I., Spiegel, A.C., Johnson, R.C., Vogelstein, J.T., et al. (2021). Visualizing synaptic plasticity in vivo by large-scale imaging of endogenous AMPA receptors. *Elife* 10, e66809. <https://doi.org/10.7554/elife.66809>.

## STAR★METHODS

### KEY RESOURCES TABLE

REAGENT or RESOURCE	SOURCE	IDENTIFIER
<b>Antibodies</b>		
Rabbit anti-EEA1 (C24B10)	Cell Signaling Technology	Cat. 3288, RRID: AB_2096811
Rabbit anti-Syntaxin13	Synaptic Systems	Cat. 100133, RRID: AB_887845
Guinea pig anti-Homer1	Synaptic Systems	Cat. 160004, RRID: AB_10549720
Rabbit anti-Synapsin	Millipore	Cat. AB1543P, RRID: AB_90757
Guinea pig anti-vGlut1	Synaptic Systems	Cat. 135304, RRID: AB_887878
Mouse anti-PAC (4D12)	Osei-Owusu et al., 2021 <sup>18</sup>	N/A
Chicken anti-MAP2	Biosensis	Cat. C-1382-50, RRID: AB_2492335
Rabbit anti-PAC	This paper	N/A
Mouse anti-Na/K-ATPase alpha (H-3)	Santa Cruz Biotechnology	Cat. SC-48345, RRID: AB_626712
Rabbit anti-GluR1	Millipore	Cat. AB1504, RRID: AB_2113602
Mouse anti-GluR2 (6C4)	Millipore	Cat. MAB397, RRID: AB_2113875
Mouse anti-PSD95 (K28/42)	UC Davis/NIH NeuroMab Facility	Cat. 75-028; RRID: AB_2292909
Mouse anti-Synaptophysin1 (7.2)	Synaptic Systems	Cat. 101011, RRID: AB_887821
Rabbit anti-Rab5 (C8B1)	Cell Signaling Technology	Cat. 3547, RRID: AB_2300649
Rabbit anti-Rab7 (D95F2)	Cell Signaling Technology	Cat. 9367, RRID: AB_1904103
Mouse anti-Rab7 (117)	Millipore Sigma	Cat. R8779, RRID: AB_882241
Rabbit anti-Rab11 (D4F5)	Cell Signaling Technology	Cat. 5589, RRID: AB_10693925
Mouse anti- $\alpha$ -Tubulin (DM1A)	Invitrogen	Cat. 62204, RRID: AB_11204167
Mouse anti-FLAG	Origene	Cat. TA50011, RRID: AB_2622345
Cy3-conjugated Streptavidin	Jackson ImmunoResearch	Cat. 016-160-084; RRID: AB_130355
<b>Bacterial and virus strains</b>		
AAV5-CaMKII-GFP-Cre	UNC Vector Core	<a href="https://www.med.unc.edu/genetherapy/vectorcore/in-stock-aav-vectors/">https://www.med.unc.edu/genetherapy/vectorcore/in-stock-aav-vectors/</a>
AAV5-CaMKII-GFP	Addgene	50469-AAV5
<b>Chemicals, peptides, and recombinant proteins</b>		
EX-Link Sulfo-NHS-SS-biotin	Thermo Scientific	Cat. 21331
NeutrAvidin Agarose	Thermo Scientific	Cat. 29202
Picrotoxin	Sigma-Aldrich	Cat. P1675
TTX	Hello Bio	Cat. HB1035
D-APV	Sigma-Aldrich	Cat. A8054
NMDA	Sigma-Aldrich	Cat. M3262
Glycine	Bio-Rad	Cat. 1610718
DHPG	Sigma-Aldrich	Cat. D3689
Biocytin	Sigma-Aldrich	Cat. B4261
Strychnine	Sigma-Aldrich	Cat. S8753
Bicuculline	Sigma-Aldrich	Cat. 14340
AcidiFluorORANGE HaloDye	Millipore	Cat. SCT212
<b>Experimental models: Organisms/strains</b>		
Mouse: <i>PACC1</i> <sup>flxed</sup>	This paper	N/A
Mouse: <i>NEX-Cre</i>	Goebel et al. <sup>31</sup>	N/A
<b>Recombinant DNA</b>		
TfR-Rph	This paper	N/A
SEP-GluA2	Richard Huganir	N/A
HaloTag-GluA2	This paper	N/A

(Continued on next page)

**Continued**

REAGENT or RESOURCE	SOURCE	IDENTIFIER
PAC-mCherry fusion	This paper	N/A
pLL3.7 shRNA control	Osei-Owusu et al. <sup>24</sup>	N/A
pLL3.7 shRNA PAC	Osei-Owusu et al. <sup>24</sup>	N/A
pLL3.7 shRNA PAC + WT hPAC	This paper	N/A
pLL3.7 shRNA PAC + YLAA hPAC	This paper	N/A
pLL3.7 shRNA PAC + K319A hPAC	This paper	N/A
hSyn-Cre-P2A-mCherry	This paper	N/A
<b>Software and algorithms</b>		
ImageJ	NIH	<a href="http://imagej.nih.gov/ij/">http://imagej.nih.gov/ij/</a>
GraphPad Prism	GraphPad Software	<a href="http://www.graphpad.com">http://www.graphpad.com</a>
pClamp 10.7	Molecular Devices	<a href="http://www.moleculardevices.com/">http://www.moleculardevices.com/</a>
Clampfit 10.7	Molecular Devices	N/A

## EXPERIMENTAL MODEL AND SUBJECT DETAILS

### Animals

All procedures related to animal care and treatment were approved by the Johns Hopkins University Animal Care and Use Committee and met the guidelines of the National Institute of Health Guide for the Care and Use of Laboratory Animals. Animals were group housed in a standard 12-h light/dark cycle with *ad libitum* access to food and water. Adult and adolescent male and female mice were used for all experiments unless otherwise stated. All mice used were generated from the C57BL/6 strain unless otherwise noted. Adolescent mice 20 to 40 days old were used for electrophysiological recordings and adult mice 3 to 5 months old were used for behavioral experiments. The *NEX-Cre* line was obtained as a gift from Klaus-Armin Nave.<sup>31</sup> *PAC*<sup>F/F</sup> mice were generated previously<sup>45</sup> and crossed with the *NEX-Cre* line to generate *PAC*<sup>F/F</sup>; *NEX-Cre* PAC cKO mice. Sprague-Dawley rats (Harlan Laboratories) were used for hippocampal or cortical cultures at embryonic day 18 (E18) as described below. All animals were group housed in a standard 12 h light/12 h dark cycle with *ad libitum* access to food and water.

### Primary neuron cultures and transfection

Primary rat neuron cultures were performed as previously described with some modifications.<sup>11</sup> Hippocampal or cortical neurons dissected from male and female E18 rat pups were plated onto poly-D-lysine coated coverslips or plates in NM5 (Neurobasal medium with 5% horse serum, 2% B27, 2 mM Glutamax, 50 U/ml penicillin and 50 mg/streptomycin). Hippocampal neurons were switched to NMO (Neurobasal medium 2% B27, 1 mM Glutamax, 50 U/ml penicillin and 50 mg/streptomycin) one day post-seeding and fed once a week with NMO. Cortical neurons were fed at day in vitro (DIV) 5 with NMO plus FDU (5 mM 5-Fluro-2'-deoxyuridine and 5 mM Uridine) to stop glia proliferation, then fed twice a week with NMO without FDU. For staining and live imaging, hippocampal neurons were plated at a density of approximately 40,000 cells/cm<sup>2</sup>. Neurons were transfected at DIV11-16 using Lipofectamine 2000 (Invitrogen) following the manufacturers protocol, and the cells were used 3–5 days later. For biochemistry, cortical neurons were plated at a high density of 100,000 cells/cm<sup>2</sup> into 6-well plates and were used at 2–3 weeks old. Primary mouse hippocampal neurons were obtained from P0 mouse pups using the same procedure and culturing conditions as rat neurons.

### Human iPSC-derived neurons

Human-iPSCs were cultured based on a previously established protocol with slight modifications.<sup>46</sup> Human-iPSCs were grown on Matrigel coated plates in Essential 8 basal medium. For stage 1 of differentiation, iPSCs were seeded in N2 medium (DMEM-F12 containing 1X N2, NEAA, and GlutaMax, 2 µg/ml Doxycycline, and 10 mM Rock inhibitor) and allowed to differentiate for 3 days with daily media changes. For stage 2 of differentiation, iPSCs were dissociated with accutase and plated onto PLO coated coverslips in complete Brainphys media (Brainphys with B-27, 10 µg/ml BDNF, 10 µg/ml NT3, 1 mg/mL Laminin, and 2 µg/ml Doxycycline). Half medium changes were performed every other day and cells were used after 14 days of differentiation. Cell lines were negative for mycoplasma contamination.

## METHOD DETAILS

### Lentivirus production and transduction

Active lentiviral particles were generated using the 3<sup>rd</sup> generation lentivirus system, consisting of pRRE, pREV, and pVSVG. Packaging vectors were co-transfected with specific lentiviral vectors into 80–90% confluent HEK293T cells using PeneFect transfection

reagent according to the manufacturers protocol. One day post-transfection, the media was replaced with DMEM supplemented with 10% FBS, 1% BSA, and 1% penicillin/streptomycin. The supernatant was collected 48–72 h after the media change and filtered through a PVDF membrane with 0.45 µm pore size. Lentivirus was concentrated using LentiX concentrator according to the manufacturers protocol and resuspended in Neurobasal medium. Lentivirus was either used immediately or kept at –80°C for long-term storage. All reagents that came into contact with lentivirus were disinfected with bleach for 24 h before disposal. The viral titer was calculated before lentiviral transduction into cultured neurons. Transduction was performed by incubating the lentivirus with neuronal cultures overnight. 100% of the media was removed the next day and replaced with 50% conditioned media and 50% fresh NMO. Cultures were used for experiments 96 h post-transduction.

### Immunocytochemistry

Neuronal cultures were fixed in 4% paraformaldehyde (PFA) and 4% sucrose (w/v) in PBS, then permeabilized with 0.1% TritonX-100 in PBS for 10 min, followed by a 30-min block in 3% BSA in PBS. Primary antibodies were diluted in blocking buffer and incubated overnight at 4C. Primary antibodies: chicken MAP2 (Biosensis C-1382-50, 1:2000), mouse hPAC (1:1000), rabbit EEA1 (Cell Signaling Technology C45B10, 1:1000), rabbit Syntaxin13 (Synaptic Systems 110-132, 1:500), mouse Rab7 (Millipore Sigma R8779), guinea pig Homer1 (Synaptic Systems 160-004, 1:500), rabbit Synapsin1 (Synaptic Systems 106-103, 1:500), guinea pig Vglut1 (Synaptic Systems 135-304, 1:500). Cells were washed with PBS and incubated with secondary antibodies conjugated to fluorescent dyes (Thermo, 1:1000) for 1 h at room temperature before final washes and mounting. Samples were imaged using a Zeiss LSM900 confocal microscope. The ImageJ plugin JaCoP was used to measure the Pearson's R correlation coefficient from co-immunolabeled images where ROIs were selected based on the fluorescence of PAC puncta.

### Live-cell imaging for endosomal pH

Primary hippocampal neurons were co-transfected with TfR-RpH and shRNA-mCherry constructs in a 1:1 ratio at DIV11 and imaged 3–5 days later. Neurons were imaged in a custom-made live imaging chamber containing ACSF at room temperature (120 mM NaCl, 5 mM KCl, 2 mM CaCl<sub>2</sub>, 1 mM MgCl<sub>2</sub>, 10 mM glucose, 10 mM HEPES, pH 7.3) to acquire basal endosomal fluorescence at 405 nm and 488 nm excitation. The chamber solution was switched to pH calibration buffers equilibrated to pH 7.5, 6.5, and 5.5. pH calibration solutions (125 mM KCl, 25 mM NaCl, 10 µM monensin, 25 mM HEPES for pH > 7.0 or 25 mM MES for pH < 7.0; pH adjusted with NaOH and HCl) were adapted from Pohlkamp et al.<sup>47</sup> Fluorescence images were acquired for both 405 nm and 488 nm stimulation for all pH solutions and were used to generate a standard curve for each experiment. Values of the 405/488 fluorescence intensity ratio from the basal ACSF condition were plotted on the standard curve to calculate pH. Imaging was performed on a Zeiss LSM900 confocal microscope.

### Live-cell imaging of SEP-GluA2 for AMPAR trafficking and chemical LTP

Primary hippocampal neurons were co-transfected with SEP-GluA2 and shRNA-mCherry constructs in a 1:1 ratio at DIV 15 and imaged at DIV 18–21 for measurements of basal AMPAR trafficking and cLTP. Live-neurons were imaged in a chamber containing ACSF at room temperature. For basal AMPAR trafficking, 2–5 dendritic spines per neuron were selected for SEP fluorescence measurement. Z-stacks were collected once per minute over a 15-min experiment measuring fluorescence intensity. Glycine-induced chemical LTP was performed as previously described with minor modifications.<sup>11</sup> Briefly, cells were pre-incubated for 1–2 h in basal ACSF (120 mM NaCl, 5 mM KCl, 2 mM CaCl<sub>2</sub>, 1 mM MgCl<sub>2</sub>, 10 mM glucose, 10 mM HEPES, pH 7.3) supplemented with 500 nM TTX, 20 µM bicuculine, and 1 µM strychnine. Baseline was collected in basal ACSF, followed by a 10 min cLTP stimulation with 200 µM glycine in the same ACSF solution but without MgCl<sub>2</sub>. Basal ACSF was used after stimulation for the remainder of imaging (50 min).

### Live-cell imaging of HaloTag-GluA2 for chemical LTD

Primary hippocampal neurons were co-transfected with HaloTag-GluA2 and shRNA-EGFP constructs in a 1:1 ratio at DIV 15 and imaged at DIV 18–21. Prior to imaging, cultures were pre-incubated in basal ACSF supplemented with 1 µM TTX for 1 h. A stock of 1mM Halo-Tag AcidifluorORANGE (Millipore Sigma, SCT212) was diluted 1:4000 in basal ACSF for dye loading at 37 °C for 15 min. Prior to imaging, AcidifluorORANGE was washed out with three washes of basal ACSF and transferred to a live-imaging chamber maintained at 37 °C and 5% CO<sub>2</sub>. For cLTD assay, neurons were stimulated for 5 min with 20 µM NMDA in ACSF with 1 µM TTX and without MgCl<sub>2</sub>, then replaced with basal ACSF for the remainder of imaging (60 min). At the end of each experiment, the solution was changed to pH 5 calibration buffer (125 mM KCl, 25 mM NaCl, 10 µM monensin, 25 mM MES) to confirm AcidifluorORANGE loading. Experiments performed under D-APV used the same experimental conditions but in the presence of 50 µM D-APV. For no-stimulation experiments, neurons were imaged for 60 min in basal ACSF, followed by pH 5 calibration buffer. Images were obtained on either Nikon Eclipse Ti2 or Zeiss 3i spinning disc microscopes with a 50 µm pinhole size. Images were processed in ImageJ-FIJI. To quantify fluorescence intensity of endocytosed AcidifluorORANGE, images were thresholded and the particle analysis function was used to obtain particle number, area, and integrated density. Integrated fluorescence intensities were plotted against baseline values to obtain fluorescence change curves (F/F<sub>0</sub>).

**Chemical LTD and surface biotinylation**

To induce chemical LTD, cultured hippocampal or cortical neurons were incubated with 50  $\mu$ M NMDA for 2 min at 37°C in culturing medium. Afterward, neurons were incubated in NMDA-free culturing medium for 15 min at 37°C. After cLTD, neurons were placed on ice for 5–10 min. Surface biotinylation was performed as previously described with some modifications.<sup>48,49</sup> Briefly, neurons were rinsed once with ice-cold PBSCM [PBS-calcium-magnesium: 1 × PBS, 1 mM MgCl<sub>2</sub>, 0.1 mM CaCl<sub>2</sub> (pH 8.0)] were incubated with Sulfo-NHS-SS-biotin (1 mg/mL, Thermo Scientific) for 20 min at 4°C. Neurons were then washed with PBSCM and incubated in 20 mM glycine twice for 5 min to quench unreacted biotinylation reagent. Neurons were lysed in lysis buffer [PBS containing 50 mM NaF, 5 mM sodium pyrophosphate, 1% Nonidet P-40, 1% sodium deoxycholate, 0.02% SDS, and protease inhibitor mixture (Roche)]. Equal amounts of proteins were incubated overnight at 4°C with NeutrAvidin agarose beads (Thermo Scientific) and then washed with lysis buffer three times. Biotinylated proteins were eluted using 2× SDS loading buffer. Surface or total proteins were then subjected to SDS/PAGE and analyzed by Western blot.

**Stereotactic surgeries**

Stereotaxic surgeries were conducted under general anesthesia using continuous isoflurane. The depth of anesthesia was monitored continuously and adjusted when necessary. Mice were fitted into a stereotaxic apparatus (RWD Life Sciences) with their heads secured by blunt ear bars. Male and female mice were injected at age 3–4 weeks. The CA1 hippocampus (bregma: −1.5 mm, lateral ±1.5 mm, ventral −2.1 mm) was injected bilaterally with 0.6  $\mu$ L of concentrated AAV using a 2.5  $\mu$ L Hamilton syringe with a 33-G needle (Hamilton) and a syringe pump (Legato 130, Kd Scientific) at 200 nL/min. Following injection, the needle was left in place for at least 10 min to slow withdrawal. AAV5-CaMKII-Cre-EGFP was obtained from UNC GTC vector core and AAV5-CaMKII-EGFP was obtained from Addgene (50469-AAV5). AAV viruses were diluted to titers of 1–3  $\times$  10<sup>12</sup> particles/ml. Mice were used for slice recording experiments at 7–14 days-post injection and GFP expression was confirmed through fluorescence microscope imaging.

**In-utero electroporation**

E15.5 pregnant PAC<sup>F/F</sup> mice were anesthetized with 1% sodium pentobarbital (0.1 mL/10g body weight) via intraperitoneal injection; then the mice were subjected to surgical procedures to expose the uterus. Each embryo was injected with 1–2  $\mu$ L of hSyn-Cre expressing plasmid DNA mixed with Fast Green into the lateral ventricle via a glass micropipette. Then, each embryo was electroporated with five 40-V pulses of 50 ms, delivered at 1 Hz, using platinum tweezertrodes in a square-wave pulse generator (BTX, Harvard Apparatus). After that, the embryos were placed back into the abdominal cavity, and the muscle and skin were sutured. Mice were placed on a 37°C-heat pad and monitored until fully awake.

**Electrophysiological recordings**

Electrophysiological recordings were performed as described previously.<sup>45</sup> Transverse hippocampal sections (300  $\mu$ m) were cut from mice (P20–P30) using a vibratome (VT-1200S, Leica) in ice-cold choline-based cutting solution containing (in mM): 110 choline chloride, 7 MgCl<sub>2</sub>, 2.5 KCl, 0.5 CaCl<sub>2</sub>, 1.3 NaH<sub>2</sub>PO<sub>4</sub>, 25 NaHCO<sub>3</sub>, 20 glucose, saturated with 95% O<sub>2</sub> and 5% CO<sub>2</sub>. Slices were transferred to artificial cerebrospinal fluid (aCSF) containing (in mM): 125 NaCl, 2.5 KCl, 2.5 CaCl<sub>2</sub>, 1.3 MgCl<sub>2</sub>, 1.3 NaH<sub>2</sub>PO<sub>4</sub>, 26 NaHCO<sub>3</sub>, 10 glucose, saturated with 95% O<sub>2</sub> and 5% CO<sub>2</sub>. The slices were allowed to recover for 1 h at 32°C and then at RT for at least 1 h before recording. All recordings were made at RT in a submerged recording chamber with constant perfusion of aCSF containing 0.1 mM picrotoxin and 0.01 mM bicuculline, saturated with 95% O<sub>2</sub>/5% CO<sub>2</sub>. Whole-cell recordings from CA1 pyramidal neurons were visualized under an upright microscope (BX51WI, Olympus) with infrared optics. Synaptic responses were recorded by 3- to 5-M $\Omega$  borosilicate glass pipettes filled with intracellular solution containing (in mM): 125 K-gluconate, 15 KCl, 10 HEPES, 1 MgCl<sub>2</sub>, 4 Mg-ATP, 0.3 Na<sub>3</sub>-GTP, 10 phosphocreatine, and 0.2 EGTA (pH 7.2, osmolality 290–300 mOsm/kg). Data was acquired with pClamp 10.7 software (Molecular Device), filtered at 1 kHz and digitized at 10 kHz. In all experiments, the series resistance (Rs) was monitored throughout the recording and controlled below 20 M $\Omega$  with no compensation. Data was discarded when the series resistance varied by  $\geq$  20%.

Miniature EPSCs (mEPSCs) were measured in the presence of 1 mM TTX and a holding potential of −70 mV. Evoked EPSCs were measured following stimulation of Schaffer collaterals with a bipolar stimulation electrode placed in stratum radiatum at the CA1 region. LTP was induced by theta burst stimulation (TBS) consisting of a single train of 5 bursts at 5 Hz, and each burst contained 4 pulses at 100 Hz. NMDAR-dependent LTD was induced by low-frequency stimulation (1 Hz, 900 s) with a holding potentiation of −40 mV, after 5- to 10-min baseline recordings. DHPG-LTD was induced by the bath application of 100  $\mu$ M DHPG for 10 min.

To measure PAC current, whole-cell recordings in hippocampal neurons transfected with PAC shRNAs was conducted as described previously.<sup>17</sup> The extracellular solution contained (in mM) 145 NaCl, 2 KCl, 2 MgCl<sub>2</sub>, 1.5 CaCl<sub>2</sub>, 10 HEPES, 10 glucose (300 mOsm/kg; pH 7.3 with NaOH). To activate PAC currents, a pH 4.6 solution was made with the same ionic composition without HEPES but with 5 mM Na<sub>3</sub>-citrate as the buffer, and pH was adjusted using citric acid. 1  $\mu$ M tetrodotoxin (TTX) and 100  $\mu$ M amiloride were added to the bath to block voltage-gated sodium channels and ASIC channels, respectively. The internal solution contained (in mM) 120 CsCl, 20 TEA-Cl, 4 MgATP, 0.3 GTP, 10 HEPES, 4 QX-314, 0.5 EGTA (290–300 mOsm/kg; pH 7.2 with CsOH). Cells were held at 0 mV and voltage ramps (minimal interval, 200 ms duration) were applied from −100 to +100 mV in 20 mV increments.

### Behavioral analysis

Open field test was conducted as previously described.<sup>45</sup> Locomotor activity was examined in adult (3–5-month-old) male mice by experimenters blinded to genotypes. The animals were placed in a chamber (18" × 18") (Photobeam activity system-San Diego Instruments) and monitored for movement by using horizontal and vertical photobeams. Beam breaks were converted to directionally specific movements and summated at 5-min intervals over 30 min. Ambulatory activity was measured as total horizontal photobeam breaks, rearing was evaluated as total vertical beam breaks.

Anxiety was assessed using an elevated plus maze (66 cm long and 5 cm wide; San Diego Instruments Inc) as described previously.<sup>50</sup> The maze consisted of two closed arms and two open arms suspended 54 cm above the ground. Immediately before testing, animals were placed, individually, into a clean cage for 5 min. Animals were placed onto the center of the elevated plus maze facing an open arm and allowed to explore for 5 min. Animal position was tracked using ANYmaze software (SD instruments).

Spatial short-term memory was tested using the Y-maze spontaneous alternation test (each arm 38 cm long, SD instruments). Mice were allowed to explore the maze for 5 min and were tracked with ANYmaze software. Spontaneous alternation was detected and calculated using ANYmaze software.

Morris water maze test was performed as previously described<sup>45</sup> with additional reversal testing. The arena consisted of a circular pool (diameter of 120 cm) filled with water that was at 24°C and made opaque with non-toxic white tempera paint. A circular, plexiglass platform (length of 10 cm) was submerged 1 cm below the surface of the water and four local cues were provided to allow spatial map generation. Mice were trained for a total of 20 trials over 5 days, with 4 trials per session and 1 session per day. Prior to the first training trial, mice were given a single habituation trial without the platform to assess any spatial bias. Trials were 60 s and mice that did not find the platform within that time were guided to the platform by the experimenter. Once on top of the platform, mice were left for an additional 10 s before being removed. Start locations (north, south, east, and west) were pseudo-randomized so that each start location was used once per session and the sequence of start locations in any session was never used twice. A probe trial was performed 24 h after the last training. Reversal training was conducted during the next 5 days with the same parameters as the acquisition training, except that the platform was placed in the opposite quadrant. A second probe trial was performed 24 h after the last reversal training. During probe trials, the platform was removed, and the mouse was allowed to swim freely for 60 s. Tracking and analysis of animal movement was done using the ANY-maze tracking system (SD instruments). Data were analyzed by comparing quadrant preferences and escape latencies averaged across animals within groups (control or cKO).

### QUANTIFICATION AND STATISTICAL ANALYSIS

Descriptions of the statistical analysis used can be found in figure legends of all figures, including the statistical test used, *n* values, and denotation of measurements including the mean and standard error of the mean (SEM).